NAVAL POSTGRADUATE SCHOOL
Monterey, California

THESIS

Simulation of Ocean Acoustic Tomography
using Matched Field Processing

by

Frédéric Strohm

June 1989

Thesis Co-Advisors: Robert H. Bourke
                           James H. Miller

Approved for public release; distribution is unlimited

REPORT DOCUMENTATION PAGE

1a REPORT SECURITY CLASSIFICATION	1b RESTRICTIVE MARKINGS
UNCLASSIFIED	

2a SECURITY CLASSIFICATION AUTHORITY	3 DISTRIBUTION AVAILABILITY OF REPORT
2b DECLASSIFICATION DOWNGRADING SCHEDULE	Approved for public release; distribution is unlimited

4 PERFORMING ORGANIZATION REPORT NUMBER(S)	5 MONITORING ORGANIZATION REPORT NUMBER(S)

6a NAME OF PERFORMING ORGANIZATION	6b OFFICE SYMBOL (If applicable)	7a NAME OF MONITORING ORGANIZATION
Naval Postgraduate School	Code 69	Naval Postgraduate School

6c ADDRESS (City, State and ZIP Code)	7b ADDRESS (City, State, and ZIP Code)
Monterey, California 93943-5000	Monterey, California 93943-5000

8a NAME OF FUNDING SPONSORING ORGANIZATION	8b OFFICE SYMBOL (If applicable)	9 PROCUREMENT INSTRUMENT IDENTIFICATION NUMBER

8c ADDRESS (City, State and ZIP Code)	10 SOURCE OF FUNDING NUMBERS			
	PROGRAM ELEMENT NO	PROJECT NO	TASK NO	WORK UNIT ACCESSION NO

11 TITLE (Include Security Classification)
SIMULATION OF OCEAN ACOUSTIC TOMOGRAPHY USING MATCHED FIELD PROCESSING

12 PERSONAL AUTHORS
Strohm, Frédéric

13a TYPE OF REPORT	13b TIME COVERED	14 DATE OF REPORT (Year, Month, Day)	15 PAGE COUNT
Master's Thesis	FROM ____ TO ____	1989, June	108

16 SUPPLEMENTARY NOTATION
The views expressed in this thesis are those of the author and do not reflect the official policy or position of the Department of Defense or the U.S. Government.

17 COSATI CODES			18 SUBJECT TERMS (Continue on reverse if necessary and identify by block number)
FIELD	GROUP	SUBGROUP	Acoustic Tomography; Matched Field Processing

19 ABSTRACT (Continue on reverse if necessary and identify by block number)

The feasibility of applying the principles of matched field processing to ocean acoustic tomography were studied under various conditions of ambient noise. Several likelihood estimators were examined (e.g., Bucker, Bartlett, Maximum Likelihood, etc.). Simulations were initially conducted for the simple case wherein only one parameter of the medium was unknown (e.g., SOFAR axis depth, surface sound speed, position of a single acoustic front). The method was then applied to the more realistic problem of locating the boundaries of an eddy in the ocean. For moderate signal-to-noise ratios, all the estimators were shown to be able to solve the problem, albeit with different efficiencies. For low signal-to-noise ratios, the MLM scheme proved to be the most reliable especially when a highly correlated ambient noise was present. In all cases, computer simulations illustrated that mismatching may occur when the parameterization of the

20 DISTRIBUTION AVAILABILITY OF ABSTRACT	21 ABSTRACT SECURITY CLASSIFICATION
☒ UNCLASSIFIED UNLIMITED ☐ SAME AS RPT ☐ DTIC USERS	Unclassified

22a NAME OF RESPONSIBLE INDIVIDUAL	22b TELEPHONE (Include Area Code)	22c OFFICE SYMBOL
Prof. Robert H. Bourke	(408) 646-3270	Code 69Bf

DD FORM 1473, 84 MAR · 83 APR edition may be used until exhausted · All other editions are obsolete

SECURITY CLASSIFICATION OF THIS PAGE

☆ U.S. Government Printing Office 1986—606-24.

UNCLASSIFIED

#19 - ABSTRACT (CONTINUED)

medium is poorly approximated. Mismatching leads to
a decrease in the efficiency of the estimators but it
may be still possible to correctly estimate the
environmental characteristics.

Accession For	
NTIS GRA&I	☒
DTIC TAB	☐
Unannounced	☐
Justification	
By	
Distribution/	
Availability Codes	
Dist	Avail and/or Special
A-1	

Simulation of Ocean Acoustic Tomography
using Matched Field Processing

by

Frederic M. Strohm
Lieutenant Commander, French Navy

Submitted in partial fulfillment of the
requirements for the degrees of

MASTER OF SCIENCE IN PHYSICAL OCEANOGRAPHY
and
MASTER OF SCIENCE IN ELECTRICAL ENGINEERING
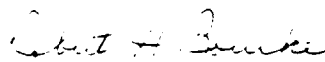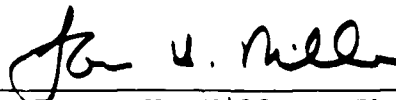
from the

NAVAL POSTGRADUATE SCHOOL
June 1989

Author: _____
Frederic M. Strohm

Approved by: _____
Robert H. Bourke, Thesis Co-Advisor

_____
James H. Miller, Thesis Co-Advisor

_____
Curtis A. Collins, Chairman
Department of Oceanography

_____
John P. Powers, Chairman
Department of Electrical and
Computer Engineering

_____
Gordon E. Schacher,
Dean of Science and Engineering

iii

ABSTRACT

The feasibility of applying the principles of matched field processing to ocean acoustic tomography were studied under various conditions of ambient noise. Several likelihood estimators were examined (e.g., Bucker, Bartlett, Maximum Likelihood, etc.). Simulations were initially conducted for the simple case wherein only one parameter of the medium was unknown (e.g., SOFAR axis depth, surface sound speed, position of a single acoustic front). The method was then applied to the more realistic problem of locating the boundaries of an eddy in the ocean. For moderate signal-to-noise ratios, all the estimators were shown to be able to solve the problem, albeit with different efficiencies. For low signal-to-noise ratios, the MLM scheme proved to be the most reliable especially when a highly correlated ambient noise was present. In all cases, computer simulations illustrated that mismatching may occur when the parameterization of the medium is poorly approximated. Mismatching leads to a decrease in the efficiency of the estimators but it may be still possible to correctly estimate the environmental characteristics.

TABLE OF CONTENTS

LIST OF TABLES

LIST OF FIGURES

ix

TABLE OF SYMBOLS

BART	Bartlett estimator
$\underline{c}$	Correlation factor of the noise at the array
BUCK	Bucker detection factor
DN	Normalized center of gravity estimator
HEIT	Heitmeyer ambiguity function
KN	Spatial autocorrelation matrix of the noise
KR	Spatial autocorrelation matrix of the replica field
KS	Spatial autocorrelation matrix of the actual field
KT	Total spatial autocorrelation matrix
MLM	Maximum Likelihood estimator
NF	Number of possible values of subscripts i and j in the construction of the replica fields
NR	Number of hydrophones at the array
$\underline{p}_j$	Complex acoustic pressure at hydrophone j
p_j	Magnitude of $\underline{p}_j$
ϕ_j	Phase of $\underline{p}_j$
$\vec{P}$	Actual acoustic pressure vector at the array
$\vec{P}'$	Replica acoustic pressure vector at the array
σ^2	Power of the noise
SNR	Signal to noise ratio
$\vec{W}$	Normalized velocity potential vector at the array

ACKNOWLEDGMENTS

I wish to thank Professor Robert H. Bourke and Professor James H. Miller for their guidance and helpful support during the research and the writing of this thesis. Our regular meetings introduced me to modern techniques of acoustical oceanography and offered me a profitable example in the conduct of a scientific research.

I am also grateful to Captain C.K. Roberts, United States Navy, for his constant advice during these two years at the Naval Postgraduate School. This dual master could not have been possible without his help and encouragement.

I thank my wife Gaelle for the patience she showed by helping me to write and correct the numerous drafts of this thesis.

Finally, I am indebted to the French Navy and the U.S. naval officers who made the presence of a French naval officer at the Naval Postgraduate School possible.

I dedicate this work to my son Kendrick.

I. INTRODUCTION

As sound waves propagate through the ocean, the complex acoustic pressure field which is generated by the source depends mainly on the path followed by the acoustic rays and the sound speed along this particular path. Due to this close relationship between the sound speed field and the acoustic pressure field, an attempt may be made to estimate the range-dependent sound speed profile (SSP) between a fixed source and an array of receivers. The characterization of the SSP from acoustical measurements generally involves inverse techniques in order to infer the acoustic properties of the medium from the pressure field measured at the receivers.

Due to the complexity of the ocean the inverse problem is most often non-linear and underdetermined. Classicial acoustic tomography solves this problem by linearization. The tomographic method is able to estimate the perturbations of the sound speed field by comparing the measured travel times of particular rays with those computed numerically from a reference sound speed field and a raytrace or a normal mode algorithm (Munk and Wunsch, 1978). The procedure provides maps of the perturbations in the sound speed field and indicates how different the actual field is from the one used as a reference. If a large enough number

1

of ray paths are used in the computations, the spatial resolution in the map of the sound speed field may be better than the one obtained from discrete CTD measurements (Howe, 1986).

Matched field processing is a different type of inverse method which was first proposed as a method to locate an acoustic source in the ocean. The principle is to compare the measured complex acoustic pressures at a vertical array with those computed from an acoustic model using various positions of the target source (Bucker, 1976). The procedure generates a function which is a measure of the likelihood between the actual acoustic pressure field created by the source (unknown position) and a replica pressure field generated from an estimate of the source location.

This study is an attempt to use matched field processing as an alternate tool to solve the inverse problem in acoustic tomography. Given the position of the source and the receivers, matched field processing is employed to compare the true complex acoustic pressures at the receiving array with the ones computed from an acoustic propagation model and various sound speed fields. Computer simulations are used to demonstrate the performance of various estimators under different signal-to-noise ratios and noise correlation matrix structures.

Chapter II provides a theoretical presentation of the likelihood estimators which are used in this study. It also illustrates how the noise is modeled and added to the simulated data. The simulations are shown in Chapter III for various conditions of noise. The first simulations deal with the simple case where only one parameter of the medium is unknown (e.g., SOFAR axis depth, surface sound speed, single frontal boundary) and where the noise is absent. The next cases are applied to the localization of an eddy in a noisy medium. Situations of both spatially uncorrelated noise and correlated noise were examined. Comparison of the estimators is provided in Chapter IV; the spreading of each likelihood function about the true value is examined in more detail under several conditions of noise power and noise correlation. Also discussed is the problem of incomplete or poor knowledge of the other environmental parameters, e.g., incorrectly specifying the bottom absorption property, and how this may introduce inconsistency in the procedure and lead to a decrease in the efficiency of the likelihood functions.

II. ACOUSTIC TOMOGRAPHY AND MATCHED FIELDS

A. PRINCIPLES OF MATCHED FIELD PROCESSING

Classical beamforming for plane waves is obtained by measuring the maximum likelihood between the actual value of the complex signal at each hydrophone and the values computed from an expected bearing (Ziomek, 1985).

In a similar fashion, the distance to a target in the near field can be estimated by comparing the actual values with those computed for different distances. The range is assumed to be correct when both sets of values correspond to the same wave front curvature (Ziomek, 1985).

Matched field processing has been used traditionally to find the location of an acoustic source in a shallow water environment. The general principle is to store the values of the received signal (amplitudes and phase) at each element of the array and then compare them with theoretical values computed for different possible positions of the target source. The true location of the emitter is determined when both fields match (Bucker, 1976; Baggeroer, Kuperman and Schmidt, 1988).

Different criteria may be used to measure the likelihood or degree of matching. Each one generates a different function which is generally well adapted for a particular

4

type of noise. Matched field detection is consistent when the medium is completely determined.

Matched field tomography deals with the inverse problem. Given that the source location is known, the purpose of the procedure is to estimate the medium characteristics, particularly the range-dependent sound speed profile. In this case, the replica or estimated fields are built from many sound speed profiles and one tries to match them with the measured one.

B. THEORY IN NOISE-FREE CONDITIONS

1. Bucker Method

According to Bucker (1976), the following "detection factor" may be used as a measure of the difference between the exact and the replica fields:

$$
BUCK = \frac{\sum_{j=1}^{NR} \sum_{k=1 \neq j}^{NR} KS_{jk} \cdot KR_{jk}}{F} \tag{2.1}
$$

where terms are defined as follows:

    KR = spatial autocorrelation matrix of one replica
         field,

    KS = spatial autocorrelation matrix of the actual
         field,

    NR = number of hydrophones in the array,

    F = scaling factor to insure a result between
         0 and 1,

<> = time average used to remove the component due
to the noise,

· = complex conjugate

The matrices KS and KR are defined by

$$KS_{jk} = p_j p_k \cdot \qquad (2.2)$$

$$KR_{jk} = p'_j p'_k \cdot \qquad (2.3)$$

where p_j and p'_j denote, respectively, the complex envelope
of the acoustic pressure and the replica pressure at
hydrophone j; similarly for hydrophone k. As demonstrated
by Bucker (1976), it is convenient to define the correlation
matrices from the complex envelopes of the signal because
the rapidly-varying time component is removed from the
computations. These complex envelopes are easily obtained
by processing the incoming signal through a classical
quadrature demodulator (multiplication by a sine wave
followed by a low-pass filter).

In the absence of noise, the time average is
unnecessary (KS is time independent) and the normalized
detection factor becomes:

$$BUCK = \frac{\sum_{j=1}^{NR} \sum_{k=1 \neq j}^{NR} KS_{jk} \cdot KR_{jk}}{(\sum_{j=1}^{NR} \sum_{k=1 \neq j}^{NR} KR_{jk} \cdot KR_{jk})^{1/2} (\sum_{j=1}^{NR} \sum_{k=1 \neq j}^{NR} KS_{jk} KS_{jk} \cdot)^{1/2}} \qquad (2.4)$$

6

This factor is similar to the classical correlation coefficient of two random variables. The expression given above does not use the diagonal elements of the matrices and can be interpreted as the output of a regular beamformer. Its value is one in the case of complete equality of the fields (KR = KS). We note also that the Bucker detection factor is one when the matrices KR and KS are proportional, as a consequence of the Schwarz inequality.

2. Heitmeyer Method

Heitmeyer (1984) defined another detection factor which he called the "source location ambiguity function." Its value is given by the following expression:

$$
HEIT = \frac{\left| \sum_{n=1}^{NR} p_n \, p_n' \right|^2}{\sum_{n=1}^{NR} \left| p_n' \right|^2}
\tag{2.5}
$$

and may be rewritten in terms of phases and magnitudes:

$$
HEIT = \frac{\left| \sum_{n=1}^{NR} p_n \, p_n' \, e^{j(\phi_n - \phi_n')} \right|^2}{NR \sum_{n=1}^{NR} p_n'^2}
\tag{2.6}
$$

It can easily be seen that the function is unnormalized. From the inequality:

$$HEIT \leq \frac{\sum\limits_{n=1}^{NR}(p_n p_n')^2}{NR \sum\limits_{n=1}^{NR}p_n'^2} \leq \frac{\sum\limits_{n=1}^{NR}p_n^2 \sum\limits_{n=1}^{NR}p_n'^2}{NR \sum\limits_{n=1}^{NR}p_n'^2} \tag{2.7}$$

an upper limit is found:

$$HEIT \leq \frac{1}{NR}\sum\limits_{n=1}^{NR}p_n^2 \tag{2.8}$$

The ambiguity function is always bounded by a quantity that may be considered as the average power detected at each hydrophone.

When the replica and the measured fields match exactly, the expression reduces to the following:

$$p'_n = p_n \tag{2.9}$$

which yields

$$HEIT = \frac{\left(\sum\limits_{n=1}^{NR}p_n^2\right)^2}{NR \sum\limits_{n=1}^{NR}p_n^2} = \frac{1}{NR}\sum\limits_{n=1}^{NR}p_n^2 \tag{2.10}$$

The inequality demonstrated previously becomes an identity when the actual and replica fields are identical.

In order to obtain a normalized ambiguity function, we divide Equation (2.6) by this upper limit.

$$HEIT = \frac{\left| \sum_{n=1}^{NR} P_n \ P_n' \ \exp(j(\zeta_n - \zeta_n')) \right|^2}{\sum_{n=1}^{NR} P_n'^2 \ \sum_{n=1}^{NR} P_n^2} \qquad (2.11)$$

3. Relation between Bucker and Heitmeyer Methods

Using the definition of the spatial autocorrelation matrix, Equation (2.4) may be written:

$$BUCK = \frac{\sum_{j=1}^{NR} \sum_{k=1 \neq j}^{NR} P_j \cdot P_j' \ P_k' \cdot P_k}{\left(\sum_{j=1}^{NR} \sum_{k=1 \neq j}^{NR} P_j' \ P_k' \ P_j' \cdot P_k' \right)^{1/2} \left(\sum_{j=1}^{NR} \sum_{k=1 \neq j}^{NR} P_j P_k \cdot P_j \cdot P_k \right)^{1/2}} \qquad (2.12)$$

If we allow the subscripts j and k to be equal, this expression becomes:

$$\frac{\sum_{j=1}^{NR} \sum_{k=1}^{NR} P_j \cdot P_k \ P_j' \ P_k' \cdot}{\left(\sum_{j=1}^{NR} \sum_{k=1}^{NR} P_j' P_k' \cdot P_j' \cdot P_k' \right)^{1/2} \left(\sum_{j=1}^{NR} \sum_{k=1}^{NR} P_j P_k \cdot P_j \cdot P_k \right)^{1/2}}$$

hence,

$$\text{BUCK} = \frac{\displaystyle\sum_{j=1}^{NR} p_j' p_j \cdot \sum_{k=1}^{NR} p_k p_k' \cdot}{\displaystyle\sum_{j=1}^{NR} p_j'^2 \sum_{k=1}^{NR} p_k^2} \qquad (2.14)$$

or, by changing the subscripts,

$$\text{BUCK} = \frac{\left|\displaystyle\sum_{n=1}^{NR} p_n p_n' \cdot\right|^2}{\displaystyle\sum_{n=1}^{NR} p_n'^2 \sum_{n=1}^{NR} p_n^2} \qquad (2.15)$$

which is exactly the normalized ambiguity function defined by Heitmeyer in Equation (2.11).

More generally, by developing the expressions of both functions, we can derive the following relation between the Bucker and Heitmeyer definitions:

$$\text{BUCK} = \text{HEIT} \cdot \frac{\displaystyle\sum_{i=1}^{NR}\sum_{j=1}^{NR} |p_i p_j'|^2}{2 \displaystyle\sum_{i=1}^{NR} p_i\, p_i'} \qquad (2.16)$$

This relation is not a simple proportionality ratio because it changes with the replica fields p'_j.

4. <u>Center of Gravity Method</u>

Other likelihood estimations can be developed using any function which has a maximum in case of perfect

matching. The center of gravity method is a procedure which solves the problem from a more mathematical viewpoint.

In the complex plane, vectors $\vec{P}$ and $\vec{P}'$ define two sets of NR points, where NR represents the number of receivers of the array. The components of the points are the real and imaginary parts of the complex acoustic pressures:

set $\vec{P}$ is composed of points $(p_i \cos \phi_i, p_i \sin \phi_i)$

set $\vec{P}'$ is composed of points $(p'_i \cos \phi'_i, p'_i \sin \phi'_i)$

In order to compute a detection factor, we calculate the euclidean distance between the centers of gravity G and G' of both sets (Figure 2.1). This distance is inversely related to the likelihood of the fields.

With a sum of weights of 1, the points G and G' are given by their coordinates:

$$X_g = \frac{1}{NR} \sum_{n=1}^{NR} p_n \cos \phi_n \tag{2.17}$$

$$Y_g = \frac{1}{NR} \sum_{n=1}^{NR} p_n \sin \phi_n \tag{2.18}$$

and

$$X'_g = \frac{1}{NR} \sum_{n=1}^{NR} p_n' \cos \phi_n' \tag{2.19}$$

$$Y'_g = \frac{1}{NR} \sum_{n=1}^{NR} p_n' \sin \phi_n' \tag{2.20}$$

11

The distance becomes:

$$D = ((X_g-X_g')^2 + (Y_g-Y_g')^2)^{1/2} \qquad (2.21)$$

or

$$D = \frac{((\sum_{n=1}^{NR} p_n \cos\phi_n - p_n' \cos\phi_n')^2 + (\sum_{n=1}^{NR} p_n \sin\phi_n - p_n' \sin\phi_n')^2)^{1/2}}{NR} \qquad (2.22)$$

We then normalize the quantity in order to obtain unity for complete matching.

$$DN = 1 - D/D_{max} \qquad (2.23)$$

where D_{max} is the largest unnormalized distance among all the replicas.

DN is only an estimation of likelihood. Although it is possible for two different sets of points to have the same center of gravity, if they are concentric, this does not occur in the simulations and the method keeps its consistency. We will see later that this distance function may lead to high secondary lobes and thus is not always reliable.

C. THEORY IN PRESENCE OF NOISE

Although it is possible to use the former expressions when noise is present which contaminates the signal, the

12

following two functions are more specifically suited for use in the presence of noise.

Johnson (1982) previously demonstrated the equivalence between the problem of bearing determination and the estimation of the spectrum of a signal. Due to this similarity, all modern spectral estimation algorithms apply equally to beamforming and matched field processing.

Although many functions may be used, as for example, MUSIC (Schmidt, 1981) or linear predictor (Johnson, 1982), we will particularly emphasize the Bartlett and Maximum Likelihood parameters which are two powerful estimators in target location problems. These estimators are especially useful in noisy conditions, because Baggeroer and his colleagues (1988) showed that they reduce to the Bucker or Heitmeyer structures when the noise is absent.

1. Bartlett Method

This method comes directly from spectral estimation theory. Baggeroer, Kuperman and Schmidt (1988) demonstrated that the power output of a Bartlett beamformer could be written in the following quadratic form:

$$BART = \vec{W} \cdot KT \; \vec{W} \qquad\qquad (2.24)$$

where $\vec{W}$ represents the normalized velocity potential vector of the replica field and KT is the total spatial correlation matrix of the signal embedded in noise.

13

Due to the proportionality between the velocity potential and the pressure field, the equivalent expression will be used:

$$\text{BART} = (\vec{P}'/|\vec{P}'|) \cdot \text{KT} \, (\vec{P}'/|\vec{P}'|)$$ (2.25)

where $\vec{P}'$ is the complex acoustic pressure vector of the replica at the array. Under the condition of perfect matching and no noise,

$$\text{BART} = \sum_{i=1}^{NR} p_i^2 = P^2$$ (2.26)

which is the summation of all signal powers among the hydrophones.

In order to normalize the function, we will divide the estimator by its largest value. For comparison between the different methods, we will focus on the width of the main lobe rather than its absolute value.

If p_i and n_i denote, respectively, the signal and the noise pressure at hydrophone i, the spatial correlation matrix has the value:

$$\text{KT}_{ij} = E((p_i + n_i)(p_j + n_j)^*)$$ (2.27)

where $E(\ )$ denotes the expectation operation.

14

When the signal and the noise are uncorrelated, the matrix reduces to the simple sum of signal and noise matrices:

$$KT_{ij} = E(p_i p_j \cdot) + E(n_i n_j \cdot) \qquad (2.28)$$

$$KT_{ij} = KS_{ij} + KN_{ij} \qquad (2.29)$$

These matrices are hermitian and at least semidefinite.

2. <u>Maximum Likelihood Method</u>

In spectral estimation, the Maximum Likelihood method, also called Capon's method or the minimum variance method, is used to compte the power spectral density of a random process (Kay, 1988). Its expression is given by:

$$P_{MV}(f) = (e^H R_{xx}^{-1} e)^{-1} \qquad (2.30)$$

where:

$$f \quad = \text{frequency,}$$

$$R_{xx} = \text{time correlation matrix of the process,}$$

$$e \quad = \text{vector whose } i^{th} \text{ component is } e^{j2^- f},$$

$$H \quad = \text{transposition of the conjugate matrix.}$$

In a similar way the output of a Maximum Likelihood beamformer is defined:

15

$$MLM = (\vec{W} \cdot KT^{-1} \vec{W})^{-1} \qquad (2.31)$$

where $\vec{W}$ and KT have previously been defined.

Following the procedure of Equation (2.25), Equation (2.31) is modified:

$$MLM = ((\vec{P'} \cdot / |\vec{P'}|) \, KT^{-1} \, (\vec{P'} / |\vec{P'}|))^{-1} \qquad (2.32)$$

In the absence of noise, KT reduces to the spatial autocorrelation of signal only, KS (Equ_ _.29)). As can be seen when the array is composed of two hydrophones, the matrix is generally singular and has no inverse. The calculation is made possible by adding a small amount of noise to the diagonal. As with the Bartlett estimator, the Maximum Likelihood factor will be divided by its largest value for normalization.
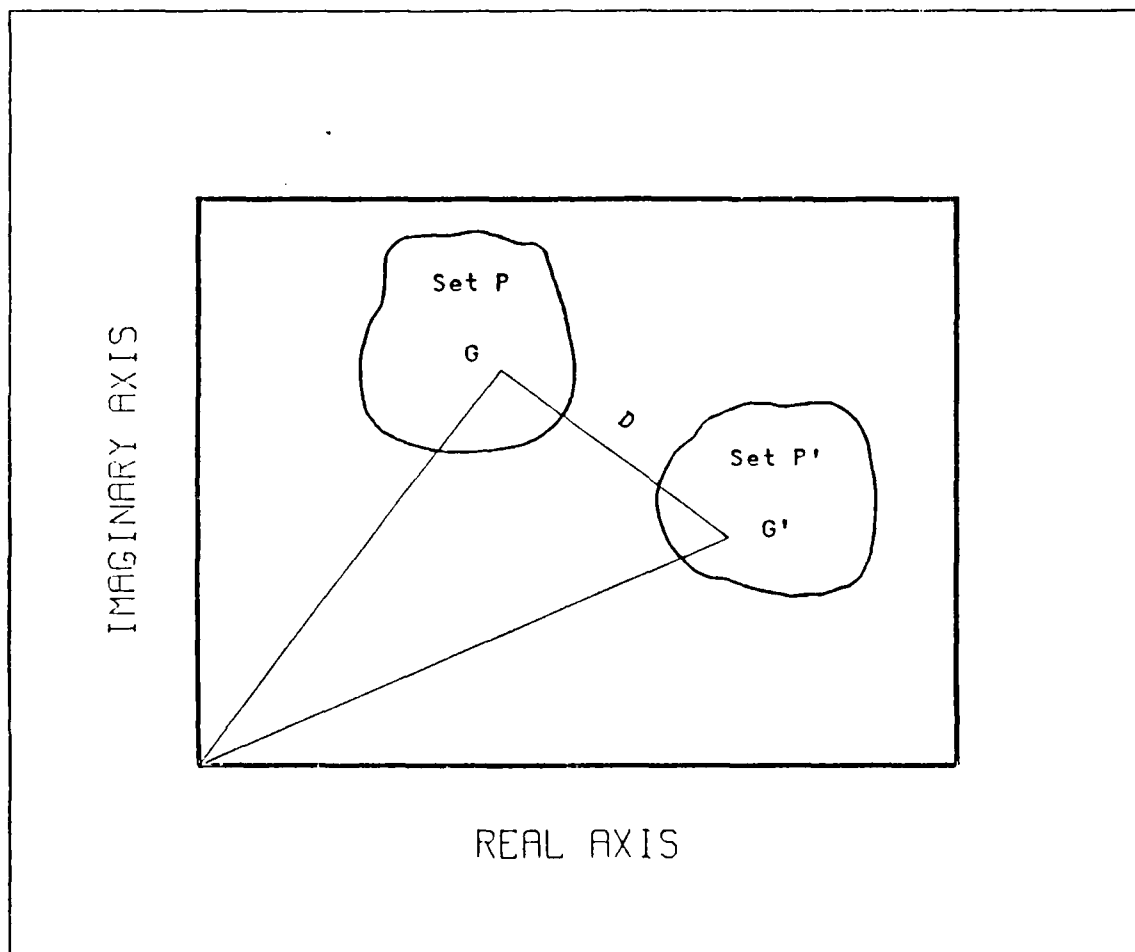
Figure 2.1   Distance Between Two Complex Sets of Points

III. SIMULATION OF ACOUSTIC TOMOGRAPHY

Matched field processing has the same form as classical beamforming. However, instead of comparing the actual field vector with a plane wave replica vector, we will try to match the actual vector with a vector computed from an acoustic propagation model. Measured data will also be simulated with the same code, then embedded or not in noise depending on the scenario under investigation.

A. PROCEDURE

1. Description of the Simulation

The receiver is modeled as a vertical array and is assumed to be composed of 20 hydrophones evenly distributed between 550 m and 1500 m. The source is located 100 km from the receiver at a depth of 1000 m. It emits a pure sine wave (tonal) centered at 100 Hz. Due to the inherent limitation of vertical angles in the parabolic approximation (Ziomek, 1985), the transmitter was selected to have a beamwidth of 40°. The bottom is 5000 m deep and is assumed to be flat and fully absorbing. This choice was made to speed up the calculations and is not a restrictive assumption. It assumes all the energy propagates by water-borne paths.

2. Acoustic Propagation Model

Several models could have been used to simulate the acoustic fields, for example, normal mode theory or the parabolic equation (PE). The PE model was used because it is more suitable for a deep water simulation; for example, an ocean bottom of 5000 m allows almost 670 propagating modes at 100 Hz and would have been computationally intensive using normal mode theory.

The classical PE approximation with split-step Fourier transform (Coppens, 1982) was available in the Environmental Acoustic Research Group package of models resident at NPS. The source code was slightly modified to save the complex acoustic pressures at the hydrophones in a file. The measured and the replica complex pressure fields were then stored in order to run the simulation programs.

3. Simulation of Noise

Noise was added to the measured data in order to produce a realistic problem and to study the behavior of the estimators in different environments. Following the procedure described by Porter, Dicus and Fizell (1987), noise was introduced by the mean of its spatial correlation matrix. This procedure is better than just altering the data with random noise because the probability density function of the noise is difficult to estimate. Moreover, all the estimators considered were written in terms of correlation matrices.

19

Ambient noise falls in two categories:

- uncorrelated noise. Its correlation matrix is proportional to the identity matrix and the proportionality factor is an indicator of the noise power.

- correlated noise. In this case the matrix has non zero terms outside the diagonal, but is nevertheless an hermitian matrix.

Several attempts to measure the coherence of ambient noise in the ocean have been conducted during the past years. One of them was made from the Trident Vertical Array and is described by Urick (1984). Figure 3.1 depicts the results of this study and has been used to generate a model of the noise correlation matrix.

The matrix was modeled in the following way:

$$KN_{ij} = \sigma^2 e^{-\beta |i-j|} \tag{3.1}$$

where σ^2 depends on the noise power and β is a factor which indicates how fast the coherence falls off outside the diagonal. The larger β is, the more uncorrelated the noise is, i.e., its spatial correlation scale becomes shorter.

Due to the spacing between the receivers in the array and the frequency (100 Hz) used in the simulation, Figure 3.1 shows that $\beta = 1.7$ is consistent with the observed ambient noise correlation.

Although the spatial correlation matrix of the noise, KN, is generally a complex hermitian matrix, the analytic modeling shown in Equation (3.1) describes a real

20

symmetric matrix. As explained by Cox (1973), this approximation is valid in the special case of zero time delay, i.e., when it is assumed that the noise is in phase among all the hydrophones of the vertical array. This assumption is relatively consistent for low frequency noise. Below 150 Hz the noise is principally due to distant shipping and arrives mainly from the horizontal.

B. ONE DIMENSIONAL PROBLEM (NOISE-FREE CONDITIONS)

In the following simulation, the shape of the sound speed profile is the only unknown. If the profile is digitized in 1 m intervals, then for a water depth of 5000 m, one would have to determine 5000 values to match the complete sound speed profile. Such a procedure would lead to an unmanageable number of computations, especially if one tries to match a large number of replica fields. However, as we are only interested in demonstrating the feasibility of the procedure, we will begin by studying the simple cases where only one or two points of the sound speed profile are unknown.

1. Determination of a SOFAR Axis Depth

We initially start with a bi-gradient sound speed profile having a sound speed minimum at 1000 m (Figure 3.2). Two replica profiles are considered wherein the SOFAR axis depth is altered by +/- 200 m (step 10 m). Note that because the surface and bottom sound speeds are unchanged,

the change in axial depth results in a change in the gradients of both the upper and lower segments of the SSP.

Three estimation techniques, the Bucker, Heitmeyer, and center of gravity methods are utilized to determine the true depth of the sound speed minimum. These estimators are computed from Equations (2.4), (2.11) and (2.23). The estimated depth of the SOFAR axis is found when an estimator shows a peak with a detection factor of 1. The results are shown in Figures 3.3, 3.4 and 3.5; each estimator demonstrates a different behavior.

The Bucker detection factor and the Heitmeyer ambiguity function both indicate a maximum at the true location of 1000 m. However a strong side lobe, centered at 1040 m, indicates these two detection factors are not robust enough to provide an unambiguous selection of the SOFAR axis depth. In addition, strong secondary side lobes are also present.

The center of gravity method (Figure 3.5) proves to be a better estimator for this situation. The main lobe is much narrower and no other lobes exist. For a noise-free ocean, this is the best estimator among the three to solve this particular problem.

2. Determination of Surface Sound Speed

In order to mimic typical seasonal or spatial changes in the SSP, the surface sound speed was permitted to fluctuate by +/- 5 m/s about a mean value (step 1 m/s). For

this situation the SOFAR axial depth was fixed at 1000 m. Hence, only the upper gradient changes as seen in Figure 3.6. We seek an estimator that will match the true surface sound speed (solid line in Figure 3.6). Using the same three estimation techniques as above, the results are shown in Figures 3.7, 3.8 and 3.9. For this situation, we observe a nearly identical behavior of the Bucker and the Heitmeyer functions, both of which have moderate side lobes at about 0.7. As before, the center of gravity estimator remains the best without any ambiguity due to the presence of secondary lobes.

3. <u>Determination of an Acoustic Frontal Boundary</u>

To model the presence of an acoustic front two different sound speed profiles are introduced, one 50 km from the other. The parabolic equation model was utilized in this range-dependent problem with the position of the front (i.e., the range at which the second SSP is encountered) allowed to vary by +/- 20 km about the true position (step 1 km). Figure 3.10 provides an illustration of the SSP setup. The Bucker and the Heitmeyer methods correctly solve this problem with relatively narrow main lobes, as shown in Figures 3.11 and 3.12. However, the center of gravity method does not perform as well (Figure 3.13). Although it is able to locate the correct value, significant sidelobes are present which could lead to an ambiguity if too small a detection threshold were chosen.

23

This last procedure is obviously not suitable for these conditions.

4. Comments on the Estimators

In order to completely appreciate the consistency of each of the previous estimators for the case where only one factor is unknown, it is important to study their response to a variety of configurations.

a. Influence of the Number of Hydrophones

In the problem of determining the depth of the SOFAR axis, the array was composed of 20 hydrophones. It is possible to run the same simulation by using only a fraction of the receivers. Plots of the Bucker estimator for four different numbers of hydrophones are shown in Figure 3.14. Although the difference is small when the number of hydrophones is reduced from 20 to five, the output of an array composed only of two receivers changes drastically. When the number of hydrophones is this small, the side lobes may have an amplitude of the same order as the main lobe, a situation which leads to full ambiguity. The number of hydrophones is thus an important parameter which must always be more than some minimum value. This value is unfortunately dependent upon the actual problem and the depth of the array relative to the axial depth. Receivers which do not intercept much of the acoustic energy can be easily omitted but those which contain significant amplitude and phase information should be retained.

b. Influence of the Frequency

Typically as a result of beamforming, the main lobe becomes narrower as the frequency of the array increases. The same phenomenon can be observed in Figure 3.15, wherein the width of the estimator peak is also a function of the frequency. However, a trade-off exists between the desired resolution (width of the detection peak) and the computation time of the PE model which increases rapidly with frequency. Also if higher frequencies (kilo-Hertz range) were used, the signal would be limited by absorption which would result in lower signal-to-noise ratios.

c. Importance of Array Position

The depth of the array is of minimal importance when working in shallow water because the entire water column is nearly insonified. Such is not the case in deep water where shadow zones exist with relatively low signal levels. Based on the depth of the source, a first guess of the depth to position the array would be to place it where the signal may be expected to occur with a high level, for example, in the vicinity of the SOFAR axis or near a convergence zone. The choice will obviously be dependent on the profile shape.

C. TWO PARAMETER PROBLEM (NOISY CONDITIONS)

    1. Localization of an Eddy

        The previous section has shown that the estimators
are generally able to find the correct value in the case of
a simple unknown and a noise-free medium. The same kind of
simulation may be run when two parameters are to be
determined. To test the ability of the various estimators
to deal with a two dimensional problem, we will examine
their ability to locate an eddy assumed to be present
between a source and a receiving array. The sound speed
profiles inside and outside the eddy are known. Thus the
only unknowns are the borders of this perturbation of the
sound field. An eddy 20 km in diameter is positioned 40 km
to 60 km from the source. The replica fields are computed
by scanning the limits from 35 km and 45 km for the border
closest to the source, and from 55 km to 65 km for the
farther boundary. Replications at 1 km interval were made.
We will thus try to match the simulated measured data with
121 replica fields. Figure 3.16 presents the true location
of the eddy in this simulation.

        Figure 3.17 shows the disposition of source and
array with regard to the energy field for the true location
of the eddy. The array lies on the SOFAR axis, almost 30 km
beyond a convergence zone. From this plot, we can expect a
high level of signal from the channel propagation and large

26

differences in phase due to multipath propagation (RR acoustic rays).

Before processing, the measured data are imbedded in noise. This noise is introduced by the spatial autocorrelation matrix described earlier. The principal assumption of this simulation is that all correlation matrices are completely known. For an actual situation, this may not be true but it is still possible to estimate the total matrix of noise from the set of measured data.

Because of its close similarity to the Bucker detection factor, the Heitmeyer function will be omitted from further analysis. The Bartlett and the Maximum Likelihood functions are introduced for these simulations, and it will later be seen that these two estimators are well suited for conditions where the signal-to-noise ratio is low.

2. Signal-to-Noise Ratio

The signal-to-noise ratio is a parameter which depends on the relative powers of the signal and the noise at the array. Following the procedure of Ziomek (1985), the signal-to-noise ratio can be written in terms of the noise-free signal and the spatial autocorrelation matrix of the noise:

$$SNR = 20 \, Log_{10} \frac{\sum_{i=1}^{NR} \sum_{j=1}^{NR} p_i p_j^*}{\sum_{i=1}^{NR} \sum_{j=1}^{NR} KN_{ij}} \qquad (3.2)$$

27

The numerator of this expression may be interpreted as the summation of all the elements of the signal spatial correlation matrix. Similarly, the denominator represents the sum of the entries of the noise correlation matrix.

The SNR was computed for several values of the noise power, σ^2, and the correlation parameter, β, that generate new values of KN_{ij} (Equation (3.1)). The results are presented in Table 3.1. The expression above shows that the SNR is reduced when the denominator of the argument increases, i.e., when the double summation $\sum_{i=1}^{NR} \sum_{j=1}^{NR} KN_{ij}$ is large due to a significant increase in the power of the noise, σ^2, or a slow decay in the correlation between the hydrophones, β. By using the results presented in Figure 3.1 and the analytic expression of the noise matrix given in Equation (3.1), the correlation of the noise will be considered high when the factor β is less than 0.57 and low when it exceeds 2.0.

TABLE 3.1

SIGNAL TO NOISE RATIO AS A FUNCTION OF σ^2 AND β

σ^2 \ β	0.57	1.0	1.7	2.0	2.2
10^{-19}	13 dB	16 dB	20 dB	21 dB	21 dB
5×10^{-19}	-1 dB	3 dB	6 dB	7 dB	7 dB
10^{-18}	-7 dB	-3 dB	0 dB	1 dB	1 dB
5×10^{-18}	-21 dB	-17 dB	-14 dB	-13 dB	-12 dB
10^{-17}	-27 dB	-23 dB	-20 dB	-19 dB	-19 dB
10^{-16}	-47 dB	-43 dB	-39 dB	-39 dB	-38 dB
10^{-18}	-67 dB	-63 dB	-60 dB	-59 dB	-58 dB

In the following sections, the performance of various estimators will be examined for several conditions, including different cases of noise power and noise correlation.

3. Bucker Detection Factor

A simulation using the Bucker detection factor was run for the case of eddy localization under both noise-free and noisy conditions.

a. Noise-free Conditions

The simulation was run by setting the power of the noise, $\cdot^2$, to zero. The autocorrelation matrix of the noise is then just the null matrix and the total matrix reduces to one of signal only, as indicated by Equations (3.1) and (2.29). A three dimensional plot and a contour plot of the detection factor are shown in Figure 3.18. The estimator is represented by a surface which has only a single maximum positioned at the correct location of the eddy. This suggests that the Bucker method is able to determine the true location of the eddy in a noise-free environment.

An interesting feature of the plot is the symmetry that exists around both diagonals of the contour. Moving on the principal diagonal, along the line:

$$Y = X + 20 \tag{3.3}$$

is equivalent to displacing an eddy with a constant diameter of 20 km. The small intervals between the contour lines along this path indicate that the location of the eddy can be determined with reasonable accuracy, once we know its diameter.

b. Case of Uncorrelated Noise

Uncorrelated noise is generated by choosing a large value of ϵ. In this case, the correlation falls off rapidly on either side of the noise matrix diagonal. For a large enough ϵ, the noise field at one hydrophone is completely dissimilar to that at another hydrophone and the noise matrix becomes diagonal. Simulations were run with $\epsilon = 10$ and different values of σ^2. All yielded the same results as in Figure 3.19, which is seen to be identical to Figure 3.18. This similarity may be explained by recalling the definition of the Bucker detection factor when noise is present:

$$
BUCK = \frac{\sum_{j=1}^{NR} \sum_{k=1 \neq j}^{NR} KT_{jk} \cdot KR_{jk}}{(\sum_{j=1}^{NR} \sum_{k=1 \neq j}^{NR} KR_{jk} \cdot KR_{jk})^{1/2} (\sum_{j=1}^{NR} \sum_{k=1 \neq j}^{NR} KT_{jk} \cdot KT_{jk})^{1/2}}
\qquad (2.4)
$$

where the total correlation matrix is given by

$$
KT_{jk} = KS_{jk} + KN_{jk}
\qquad (2.29)
$$

or,

$$KT_{jk} = KS_{jk} + \sigma^2 \exp(-\beta|j-k|) \qquad (3.4)$$

As can be seen, this expression only uses the cross terms of the matrix. When β is large enough, the second term in the right hand side of Equation (2.29) is almost negligible for every value of the noise power, σ^2; thus the cross terms of the total matrix KT reduce to the cross terms of the correlation matrix of the signal KS.

$$KT_{jk} \approx KS_{jk}, \quad j \neq k \qquad (3.5)$$

By changing the value of σ^2, the power of the noise is modified, but the new diagonal terms do not play a role in the calculations. The Bucker detection factor is thus insensitive to perfectly uncorrelated noise; in this case, the performance is exactly identical to the one in noise-free conditions.

c. Case of Uncorrelated Noise

Any combination of noise power, σ^2, and noise correlation, β, yields a different pattern of the detection factor. In cases for which the spatial correlation of the noise is high, the Bucker method may still be able to maximize the detection factor at the correct location, but the absolute value of the peak will decrease as the

31

ambiguity surface becomes flatter. Figure 3.20 illustrates this type of behavior.

Whenever both β and σ^2 generate a low signal-to-noise ratio (large power, σ^2, or small correlation parameter, β), the procedure fails and the localization of the eddy becomes impossible (see Figure 3.21). We will quantify the effects of σ^2 and β on localization below.

4. Bartlett Estimator

The same simulations as above were run using the Bartlett estimator under noise-free and noisy conditions.

a. Noise-free Medium

In a generic noise-free environment, the performance of the Bartlett estimator is similar to the Bucker detection factor, as shown in Figure 3.22. As expected, the same symmetry along the diagonals is still present.

b. Correlated Noise

The performance of the Bartlett estimator changes significantly as σ^2 and β vary. Figure 3.23 provides an example of the plot for $\sigma^2 = 10^{-16}$ and $\beta = 1.7$, where the true location is found. Figures 3.24 and 3.25 illustrate failures of the method due to a weak signal-to-noise ratio brought about by strong noise and highly correlated noise, respectively. It will later be established that the usual characteristics of the noise in a deep ocean do not generally lead to this kind of ambiguity.

5. Maximum Likelihood Method

The MLM estimator was calculated using the same noise conditions as for the Bartlett function. An examination of noise-free conditions is not possible because of the singularity of the correlation matrix. Equation (2.31) shows that the expression of the Maximum Likelihood estimator requires the calculation of the inverse matrix KT^{-1}.

$$MLM = (\bar{W} \cdot KT^{-1} \bar{W})^{-1} \qquad (2.31)$$

When noise is absent, the matrix KT reduces to the correlation matrix of the signal KS which is generally singular.

a. Slightly Correlated Noise

When $-^2 = 10^{-16}$ and $= 1.7$, the method gives better results than the Bartlett estimator with relatively low side lobes (compare Figure 3.26 with Figure 3.23).

b. Strongly Correlated Noise

With a more highly correlated ambient noise ($= 0.17$), as depicted in Figure 3.27, it is still possible to obtain a correct location of the eddy. By comparing this plot with Figure 3.25, we note that the Bartlett estimator was unsuccessful in this case. Nevertheless, even for the MLM technique, a very low signal-to-noise ratio will result in a failure as shown in Figure 3.28.
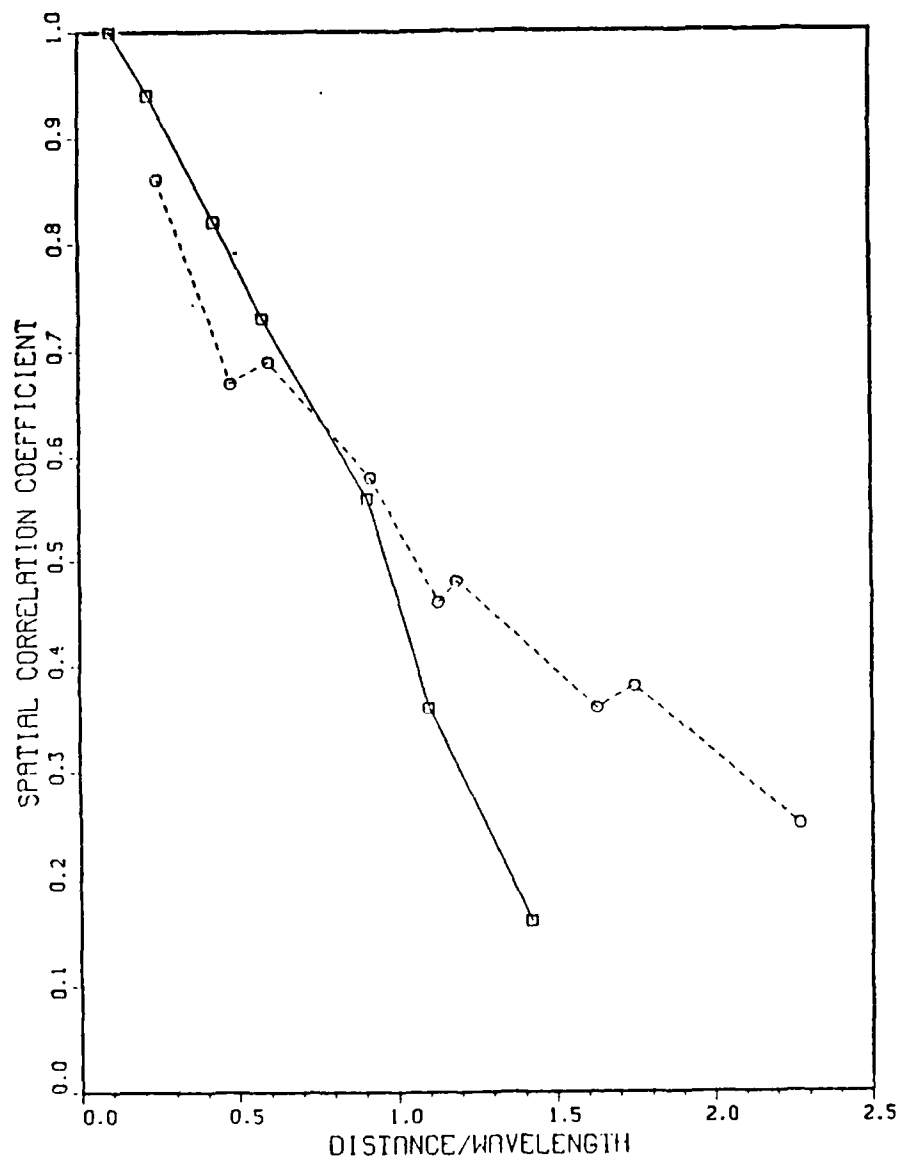
Figure 3.1   Spatial Correlation of Ambient Noise for
        Frequencies 50-100 Hz (____) and 200-400 Hz
        (---)
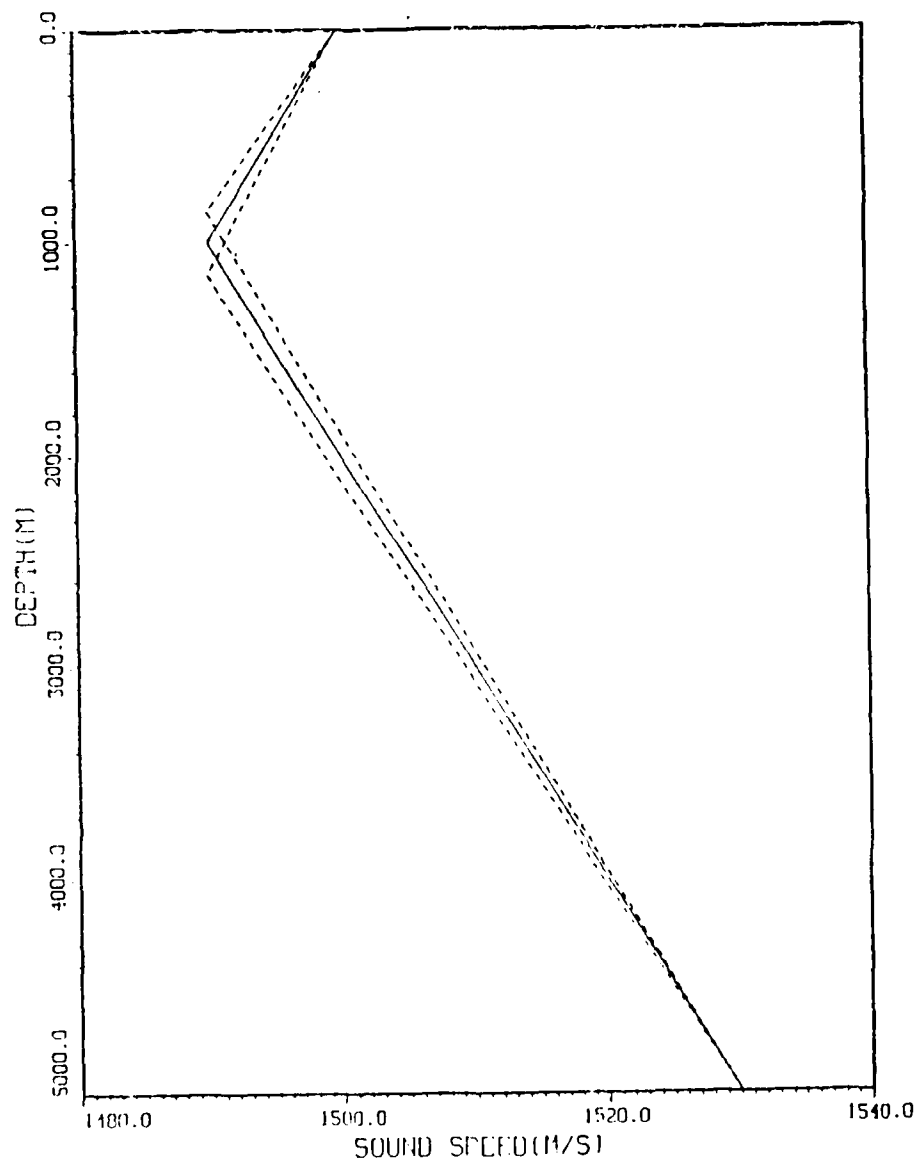
Figure 3.2   Actual and Extreme Replicas of the SSP used
              in the Simulation to Determine SOFAR Axis
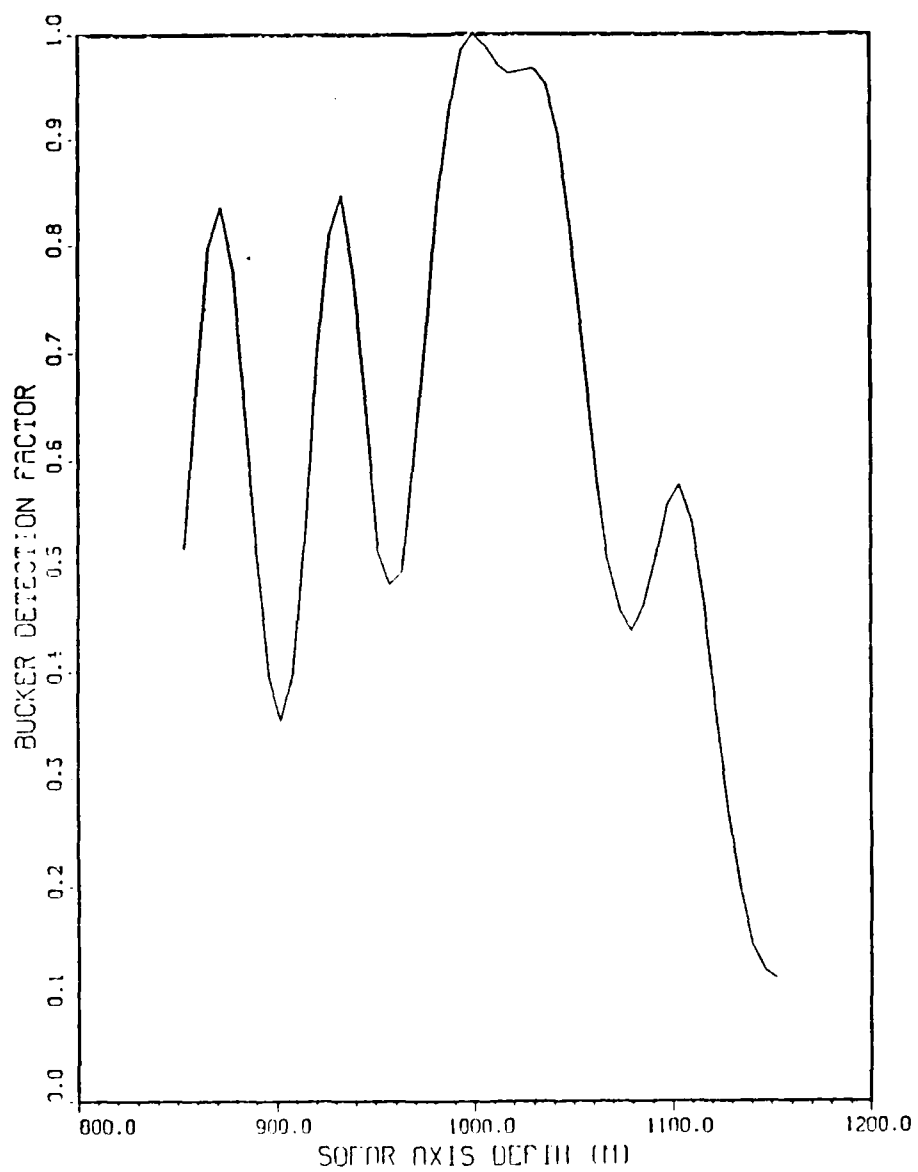   Depth

35

Figure 3.3 SOFAR Axis Depth Determination. Bucker
- Detection Factor

36
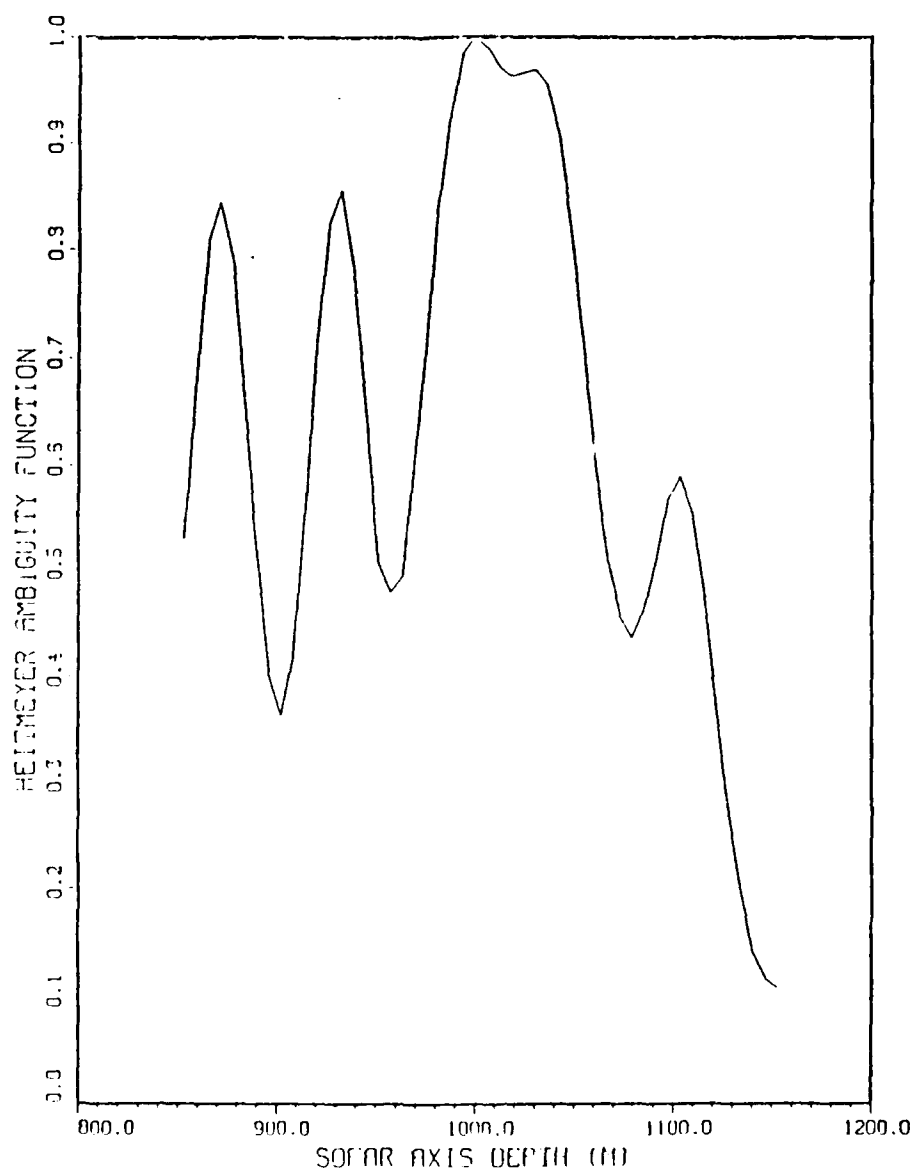
Figure 3.4 SOFAR Axis Depth Determination. Heitmeyer
            - Ambiguity Function
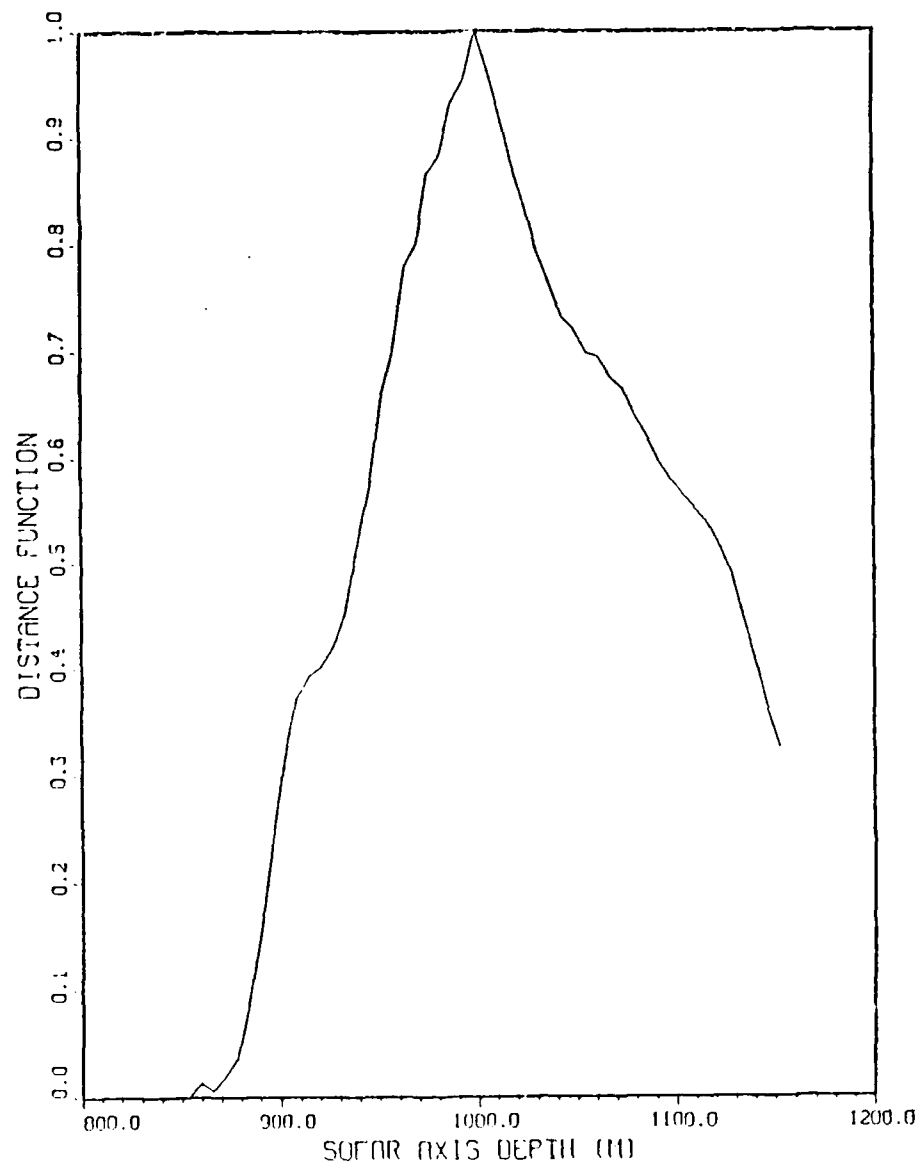
Figure 3.5   SOFAR Axis Depth Determination.   Center
. of Gravity Method

38
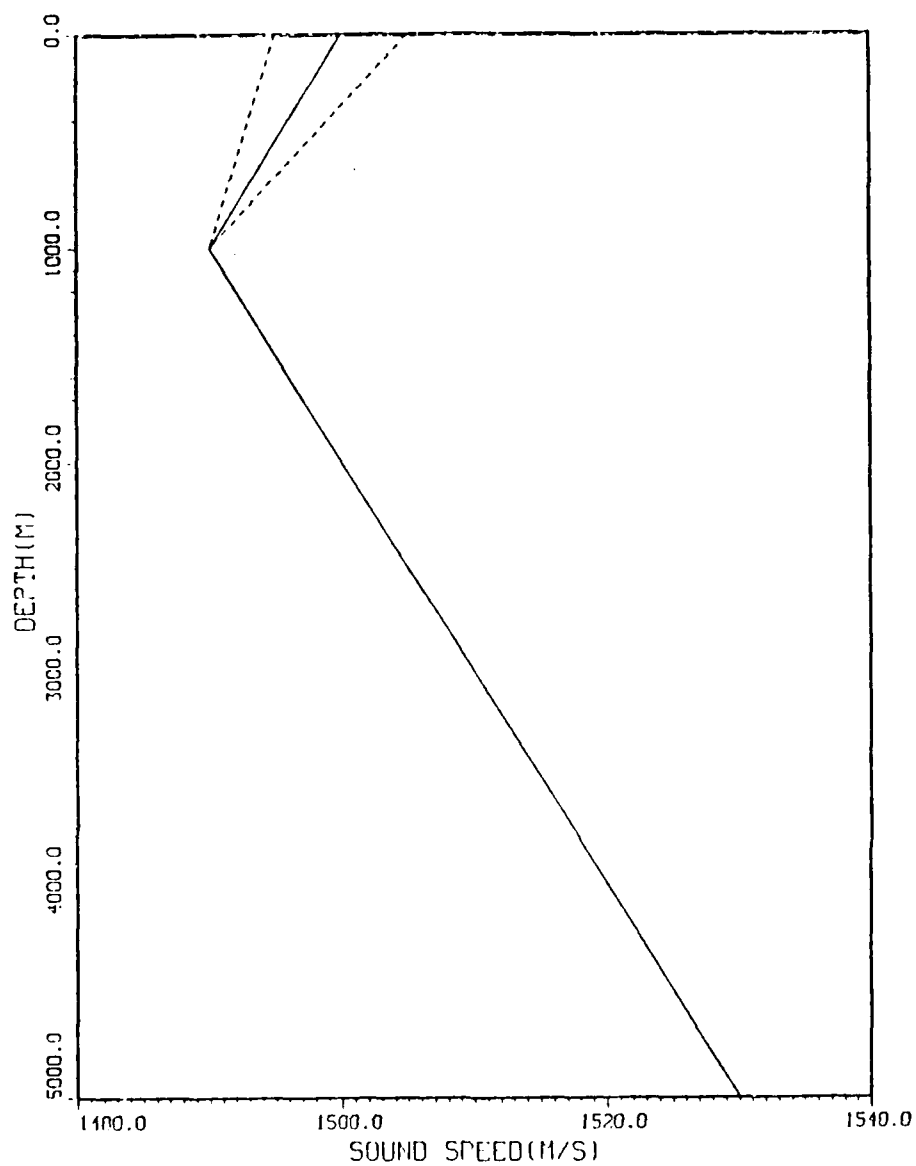
Figure 3.6   Actual and Extreme Replicas of the SSP used
             in the Simulation to Determine the Surface
             Sound Speed

39
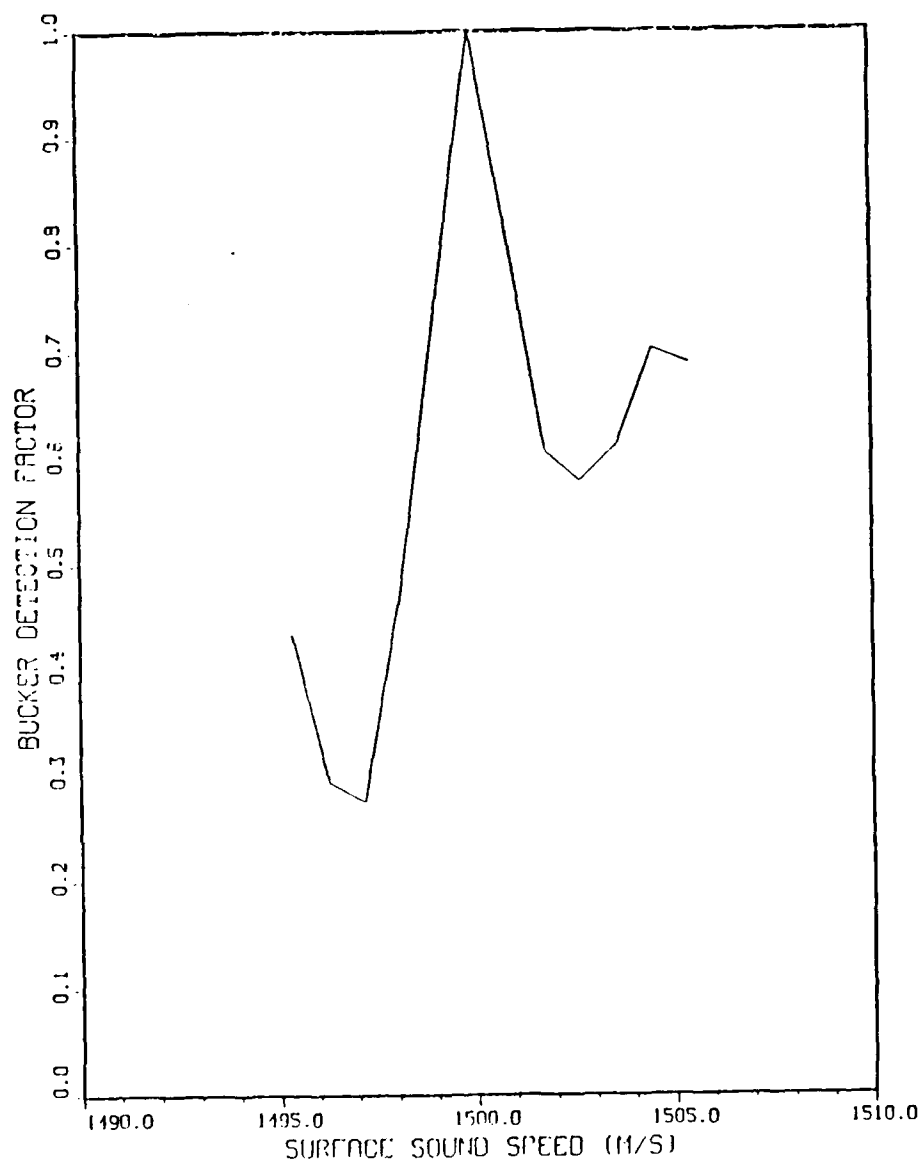
Figure 3.7   Surface Sound Speed Determination.   Bucker
   -   Detection Factor
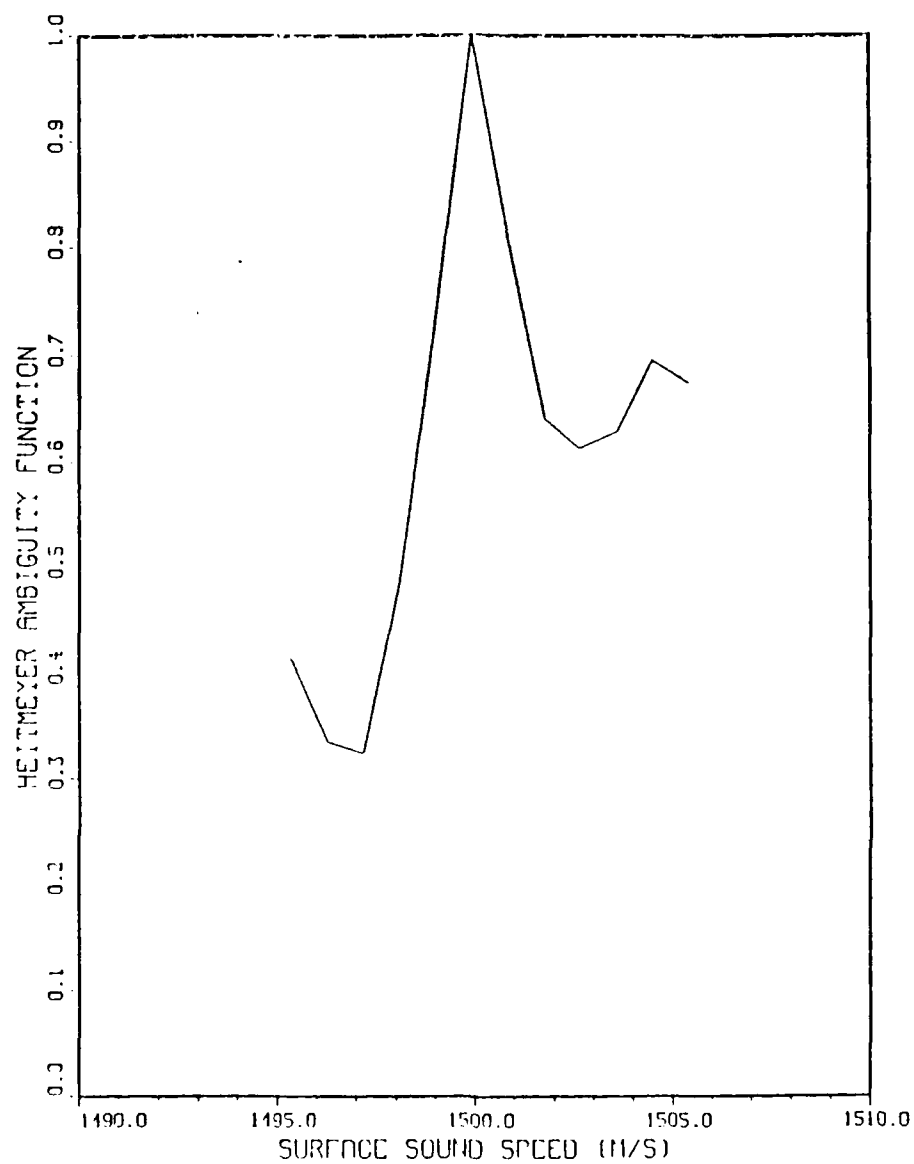
Figure 3.8   Surface Sound Speed Determination.
              Heitmeyer Ambiguity Function
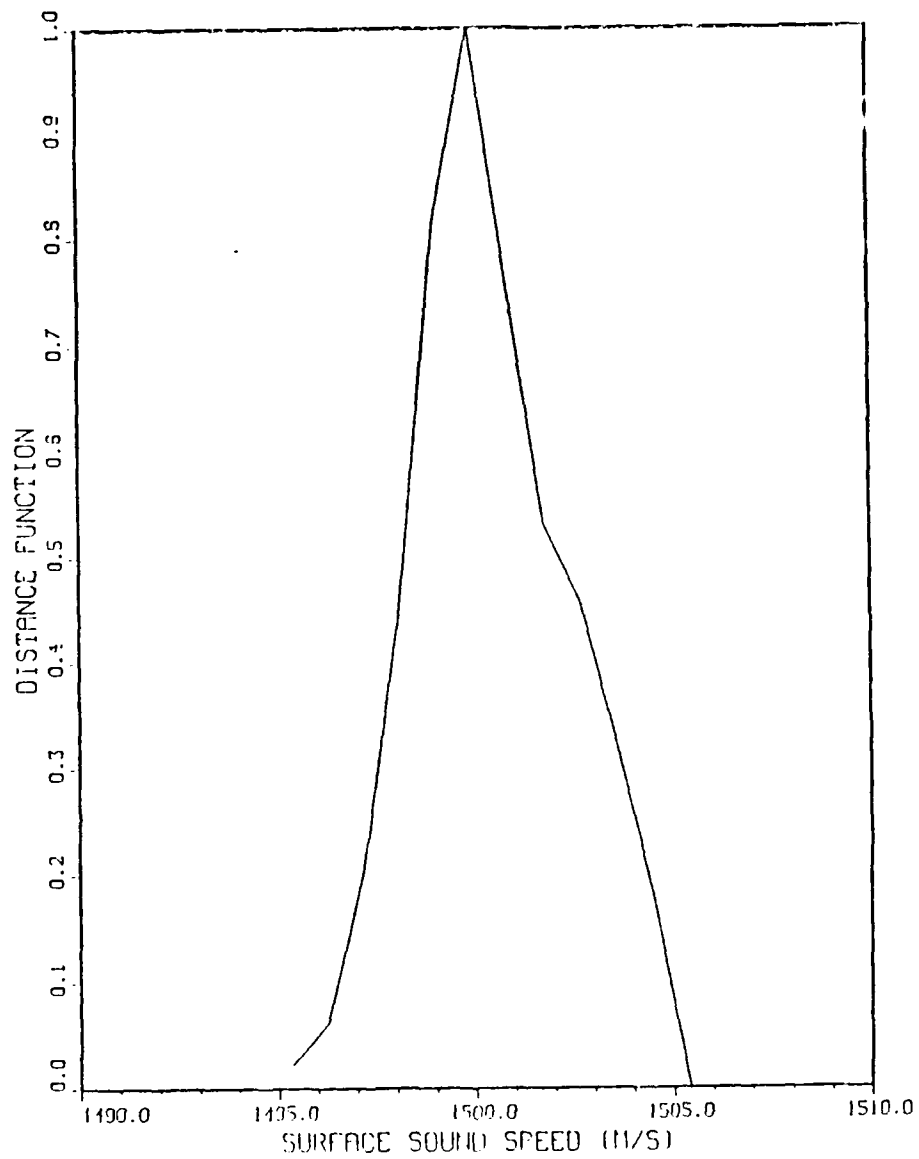
Figure 3.9   Surface Sound Speed Determination.   Center
  -     of Gravity Method
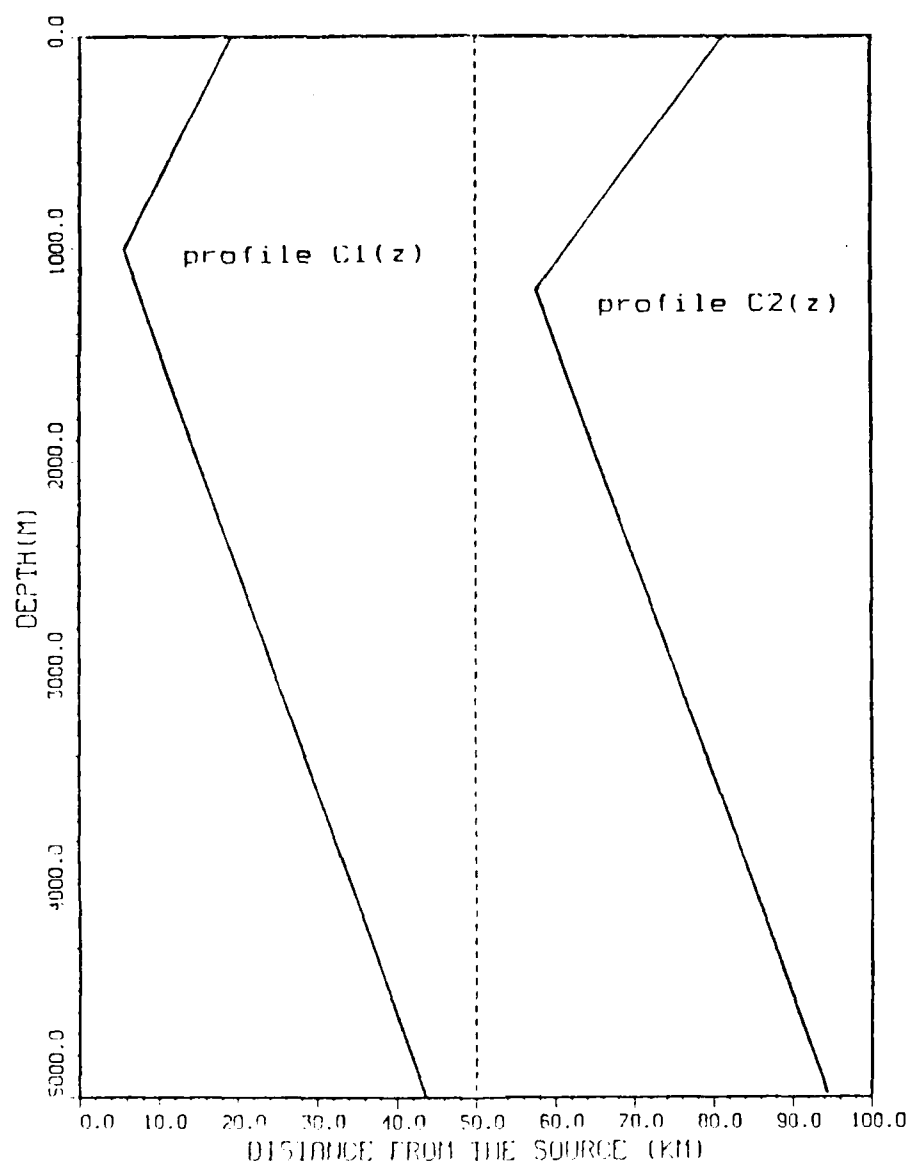
Figure 3.10   Simulation to Determine the True Location
         of an Acoustic Front
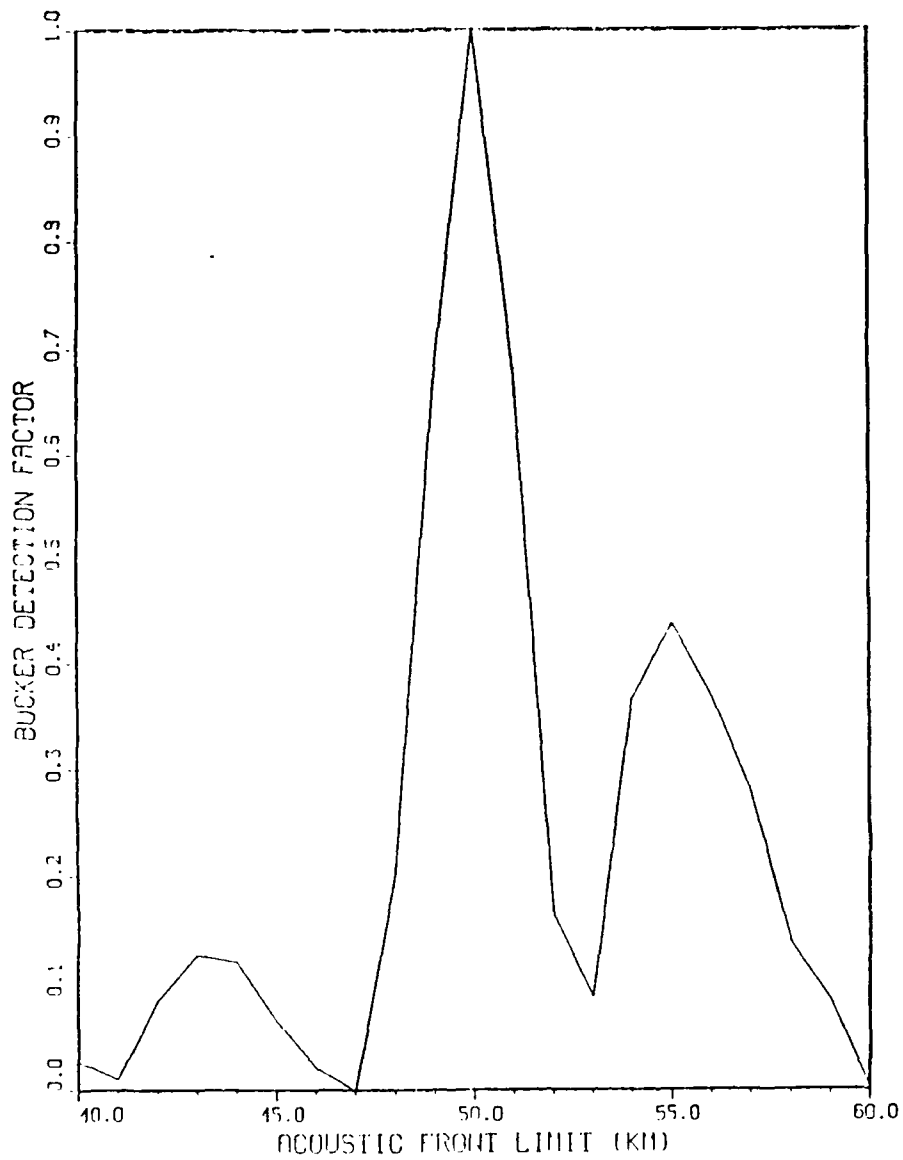
Figure 3.11 Acoustic Front Determination. Bucker
            Detection Factor

44
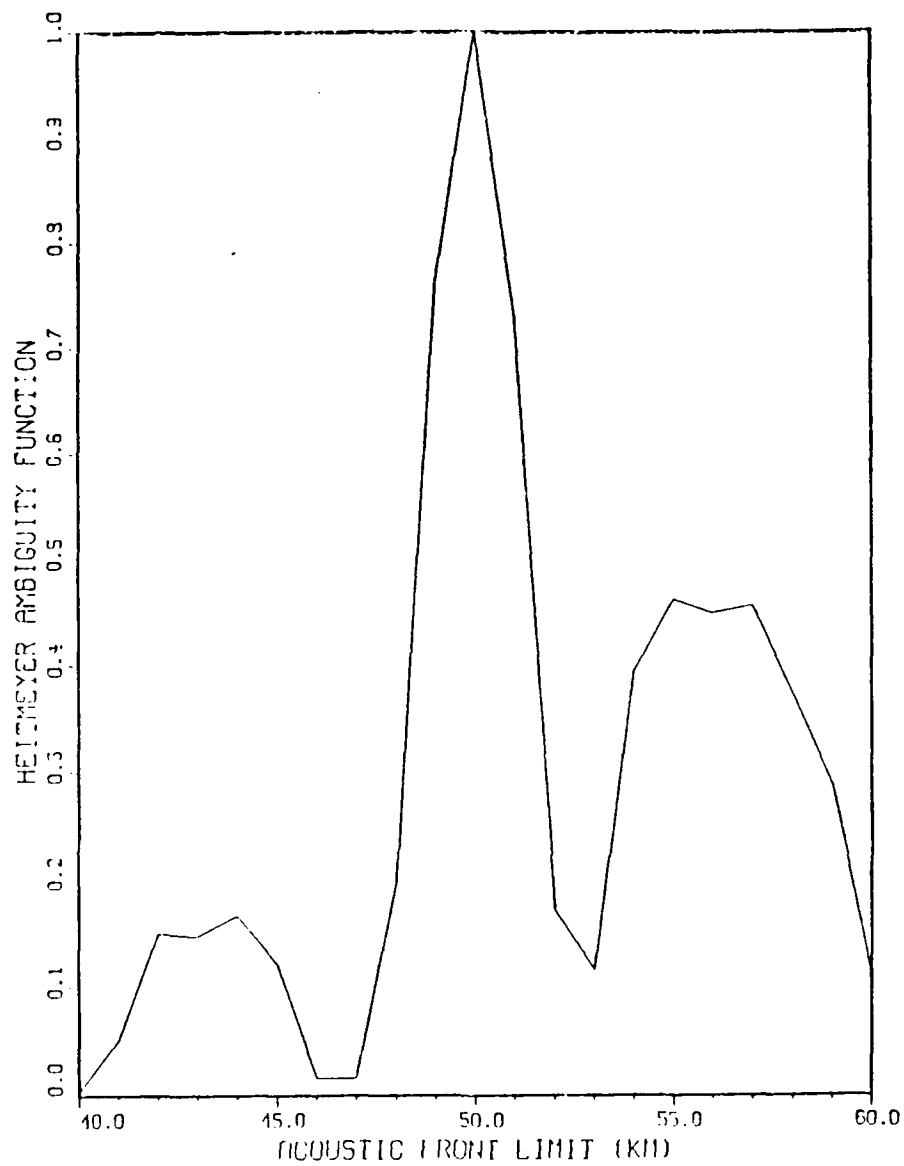
Figure 3.12 Acoustic Front Determination. Heitmeyer
         Ambiguity Function
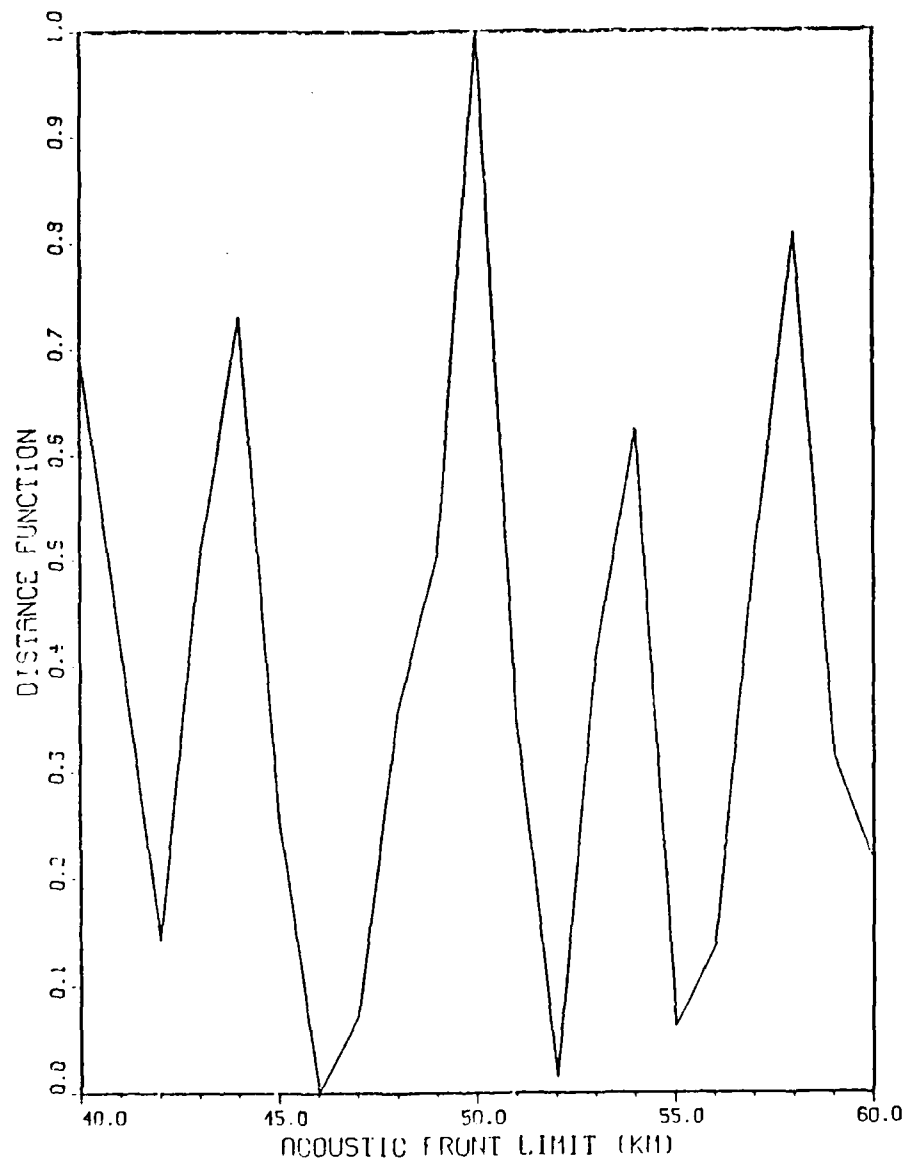
Figure 3.13   Acoustic Front Determination.   Center
        -        of Gravity Method

46
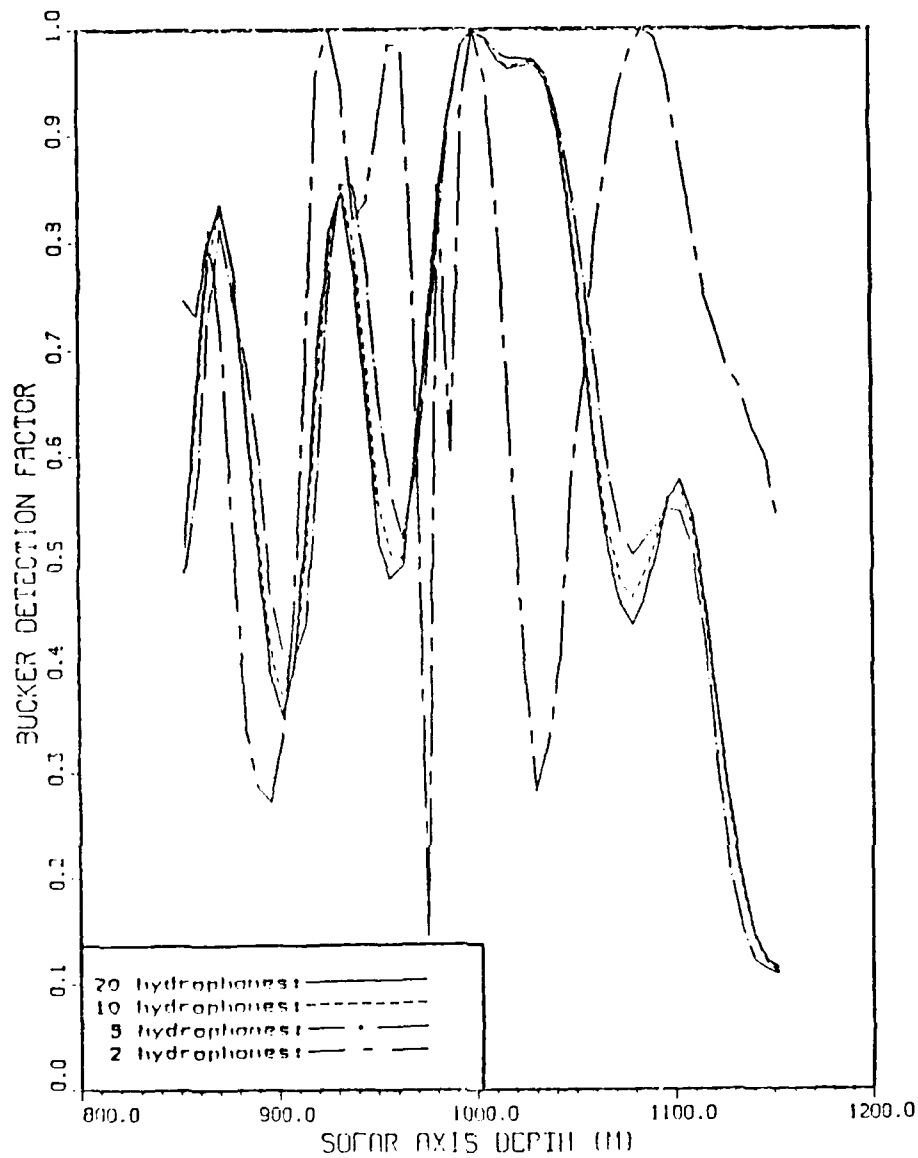
Figure 3.14   SOFAR Axis Depth Determination for Various
-    Numbers of Hydrophones in the Array

47
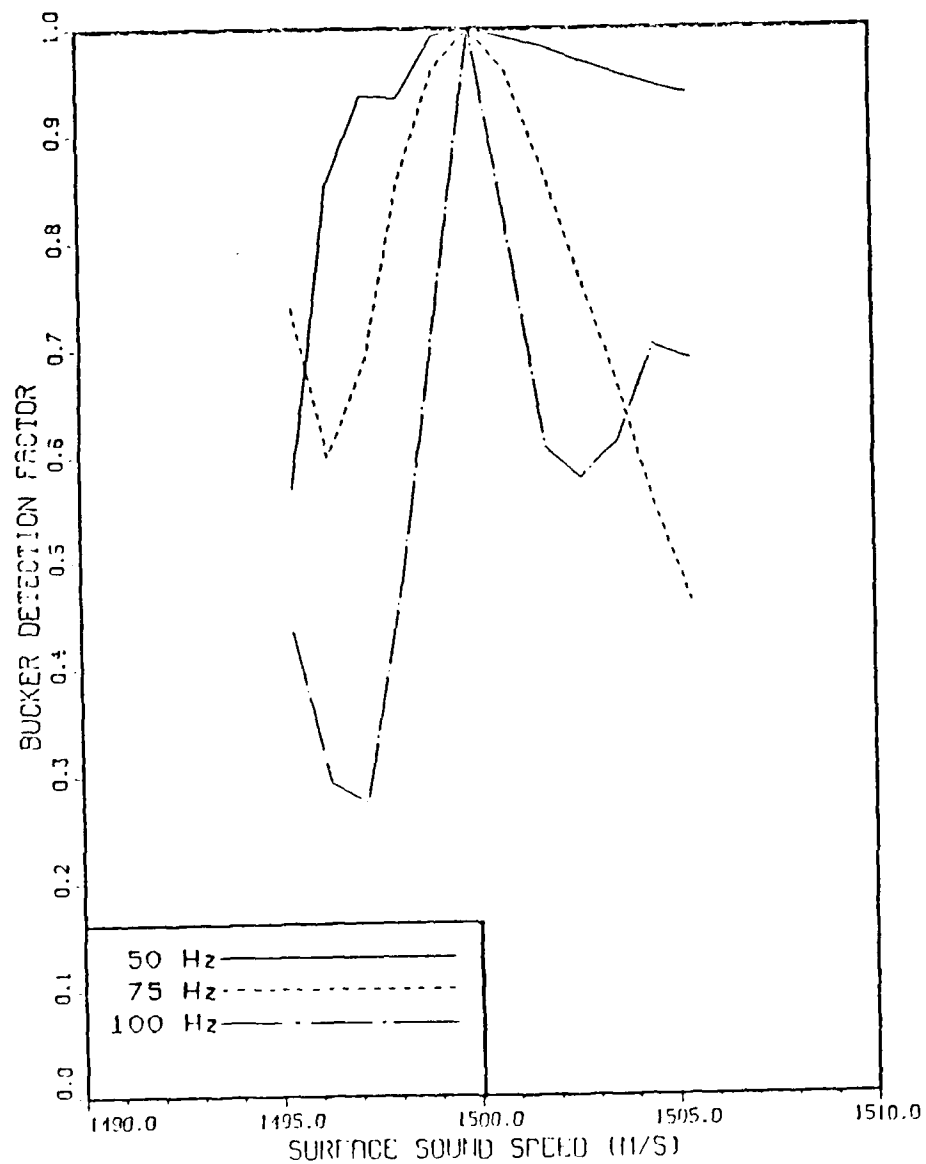
Figure 1.15   Surface Sound Speed Determination.
—   Influence of the Frequency of the Source
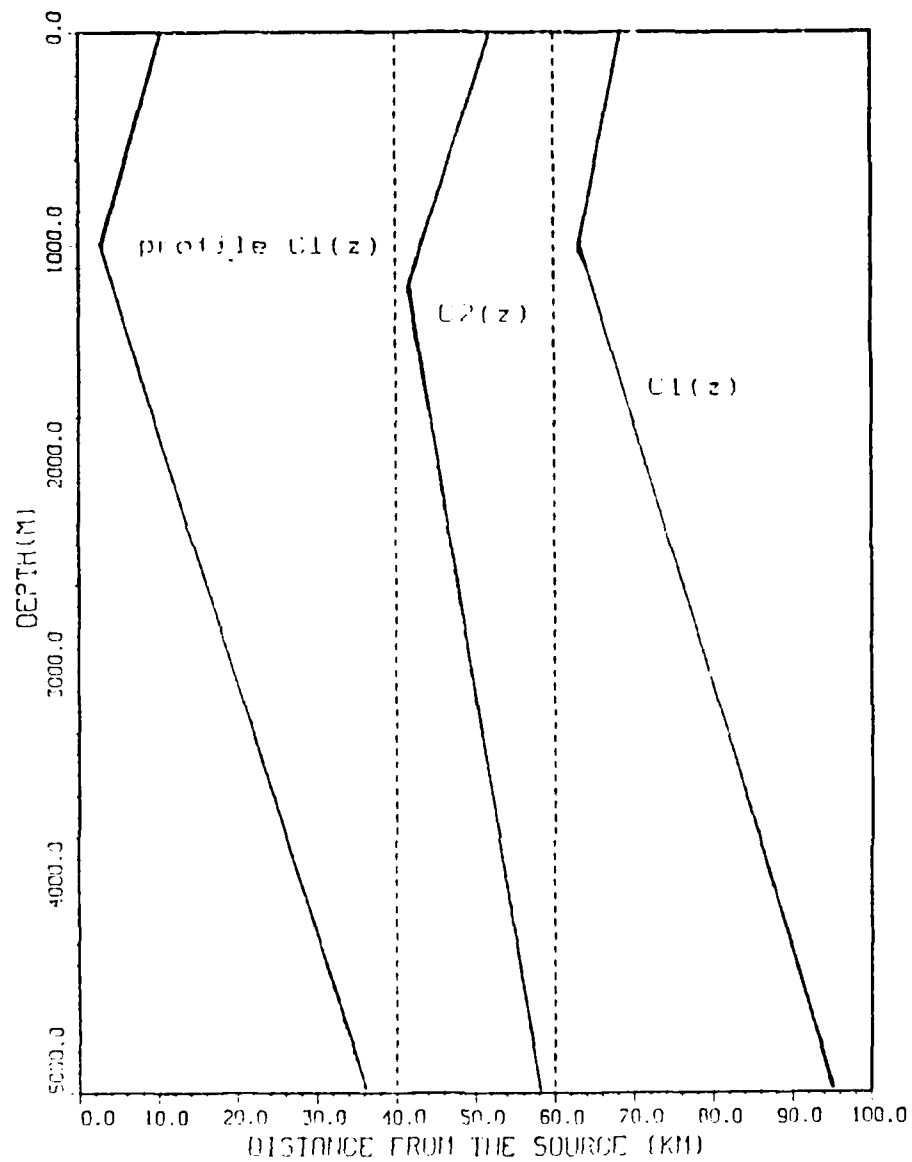
Figure 3.16   Eddy Localization.   True Position (---)
of the Eddy Boundaries
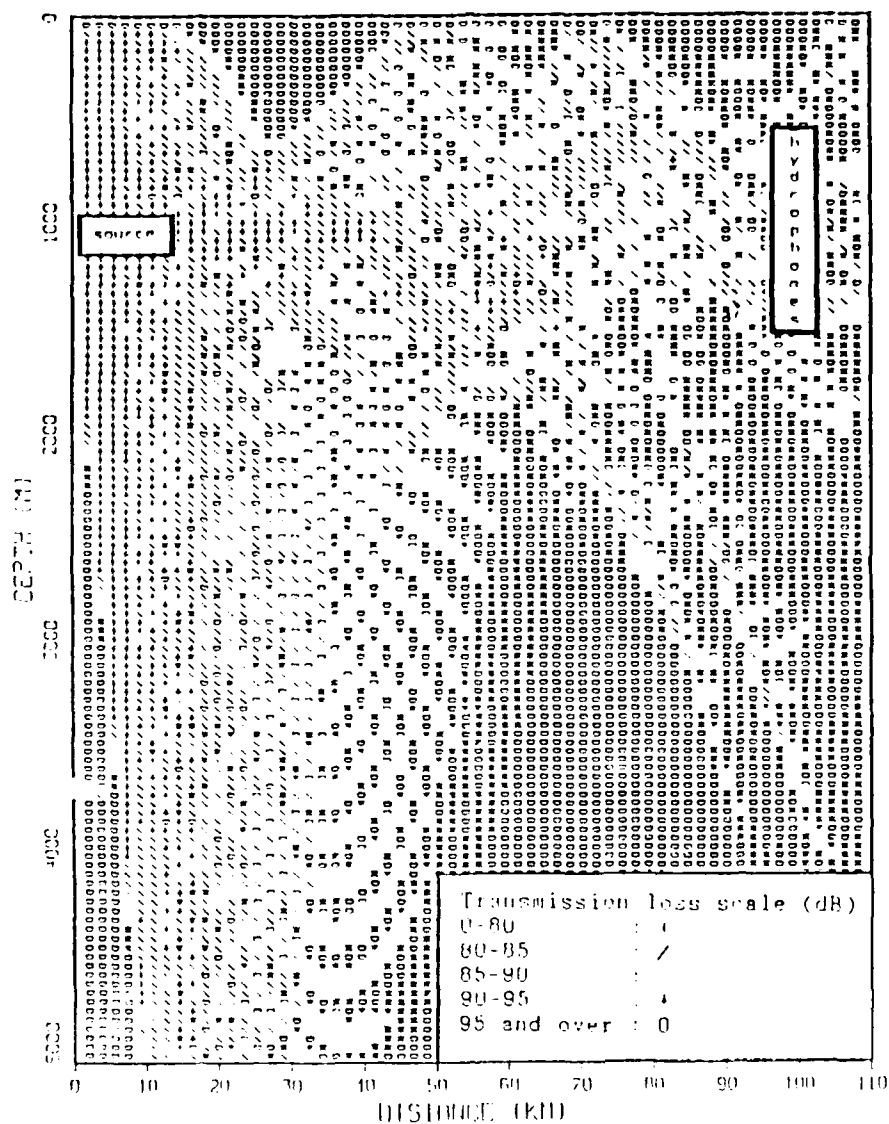
Figure 3.17   Eddy Localization.   Energy Field for the
             True Location of the Eddy
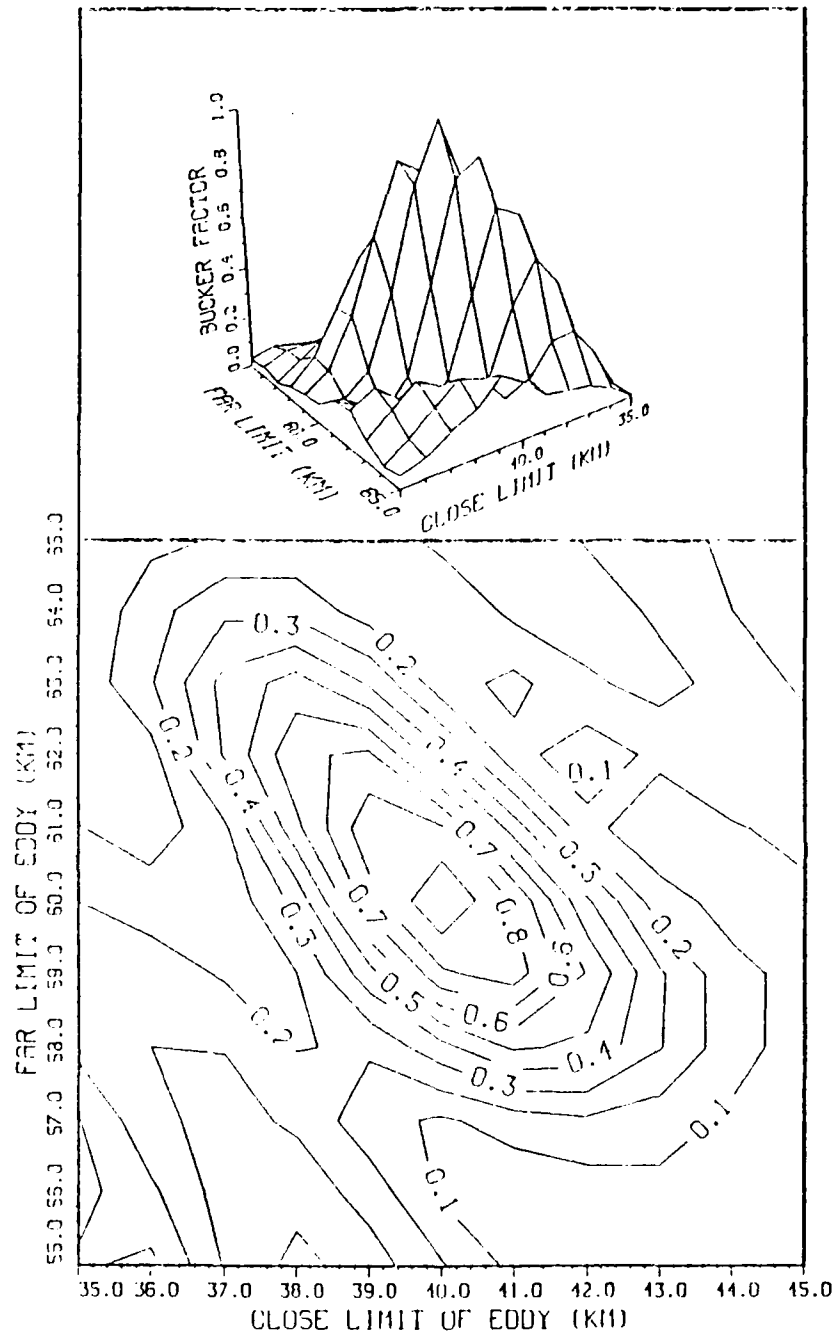
Figure 3.18   Eddy Localization.   Bucker Detection
              -    Factor.   Noise-Free Conditions

51
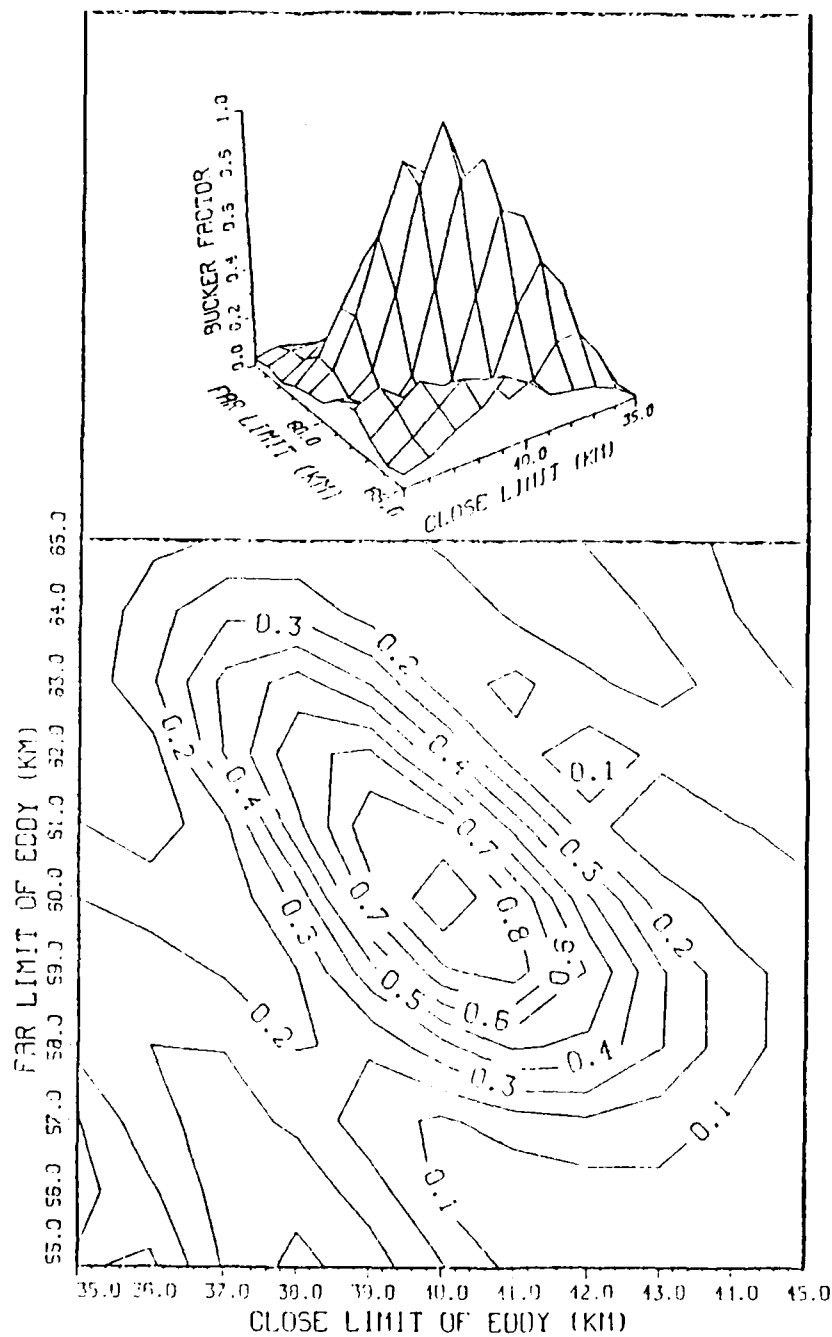
Figure 3.19   Eddy Localization.   Bucker Detection Factor
-           Illustrating Condition of Uncorrelated
             Noise and Moderate Noise Power, $\sigma^2 = 10^{-16}$,
             $\beta = 10$
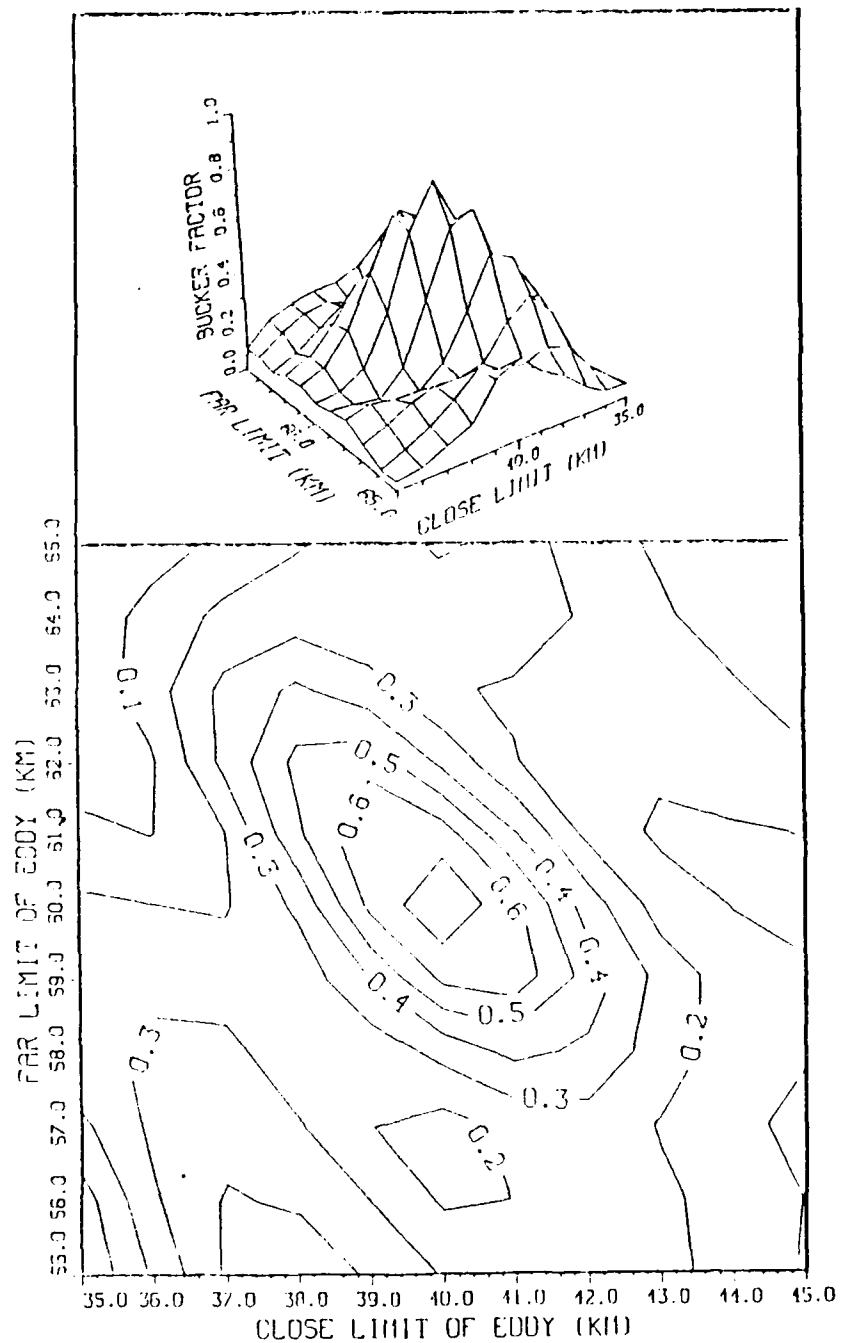
Figure 3.20   Eddy Localization.   Bucker Detection Factor
Illustrating Condition of Highly Correlated
Noise and Moderate Noise Power, $\sigma^2 = 10^{-17}$,
$\rho = 0.15$

53
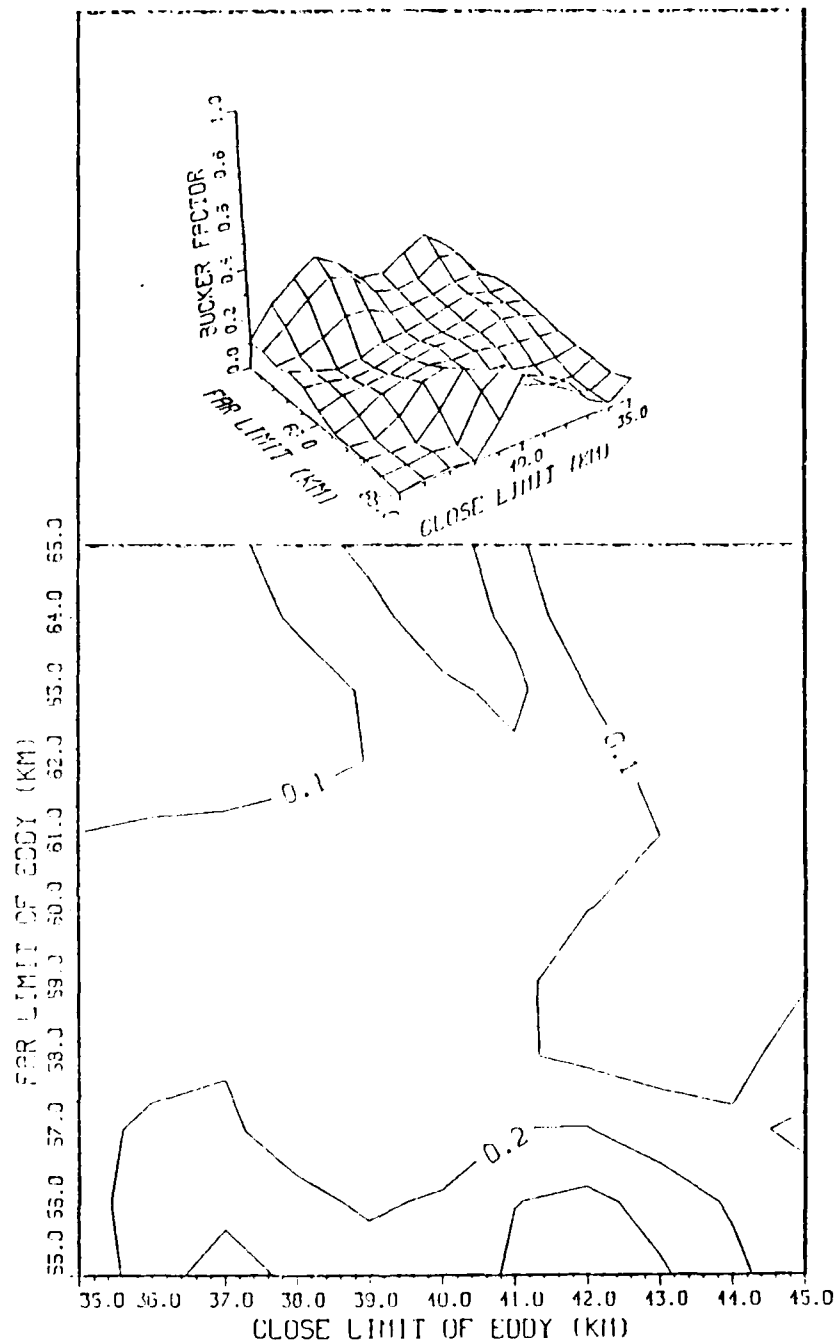
Figure 3.21 Eddy Localization. Bucker Detection Factor
Illustrating Condition of Highly Correlated
Noise and Strong Noise Power, $\sigma^2 = 10^{-16}$,
$\beta = 0.15$
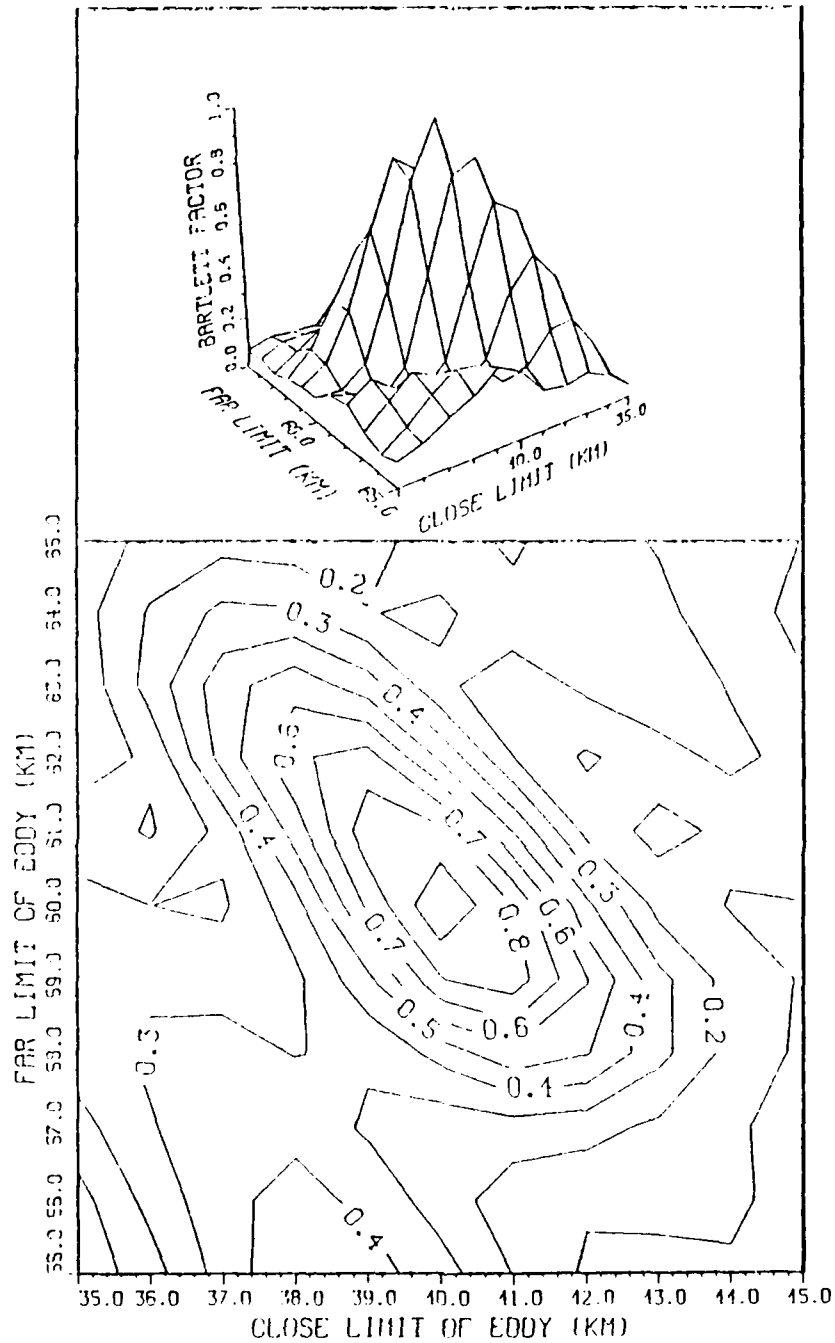
Figure 3.22 Eddy Localization. Bartlett Estimator.
- Noise Free Conditions
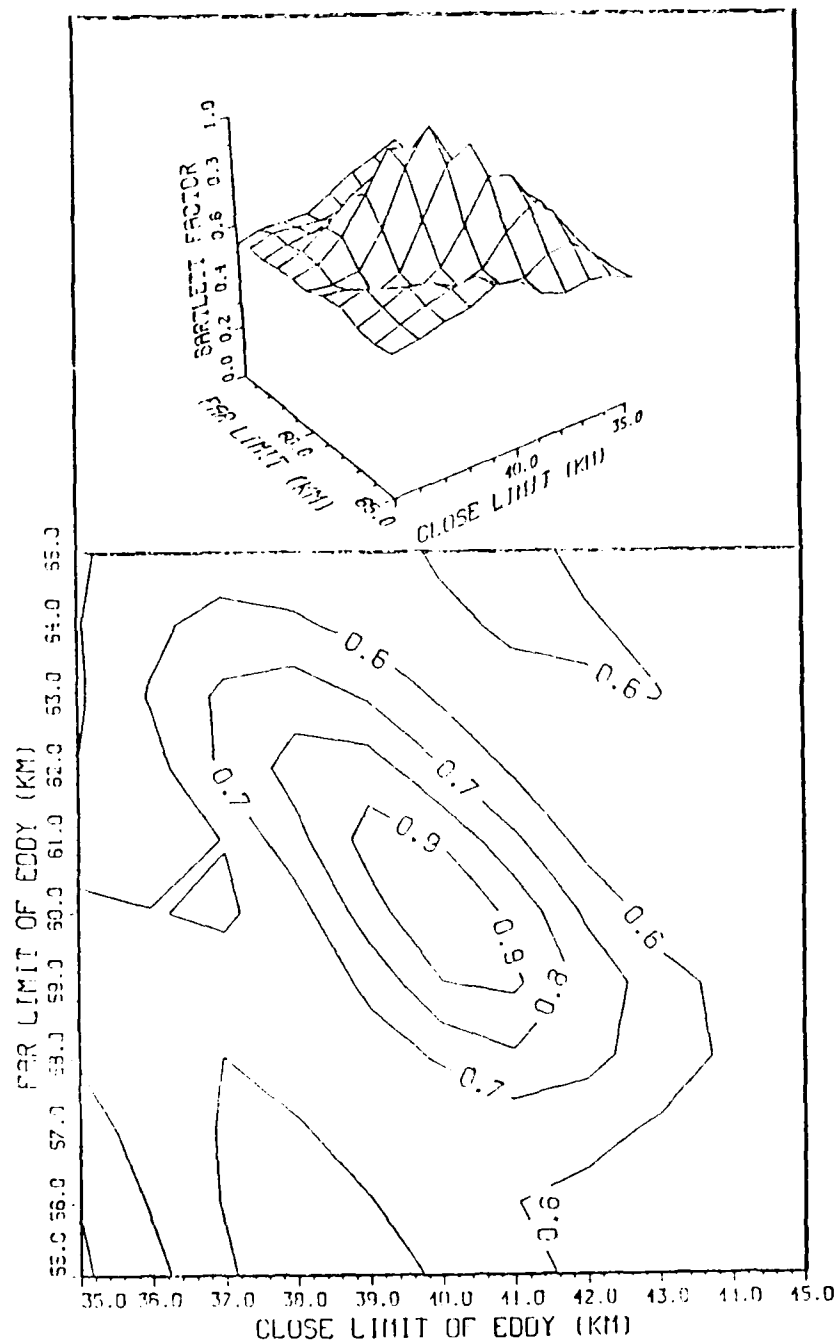
Figure 3.23   Eddy Localization.   Bartlett Estimator
        -   Illustrating Condition of Moderate Noise
            Power and Moderate   Noise Correlation,
            $\sigma^2 = 10^{-16}$, $\beta = $?

56
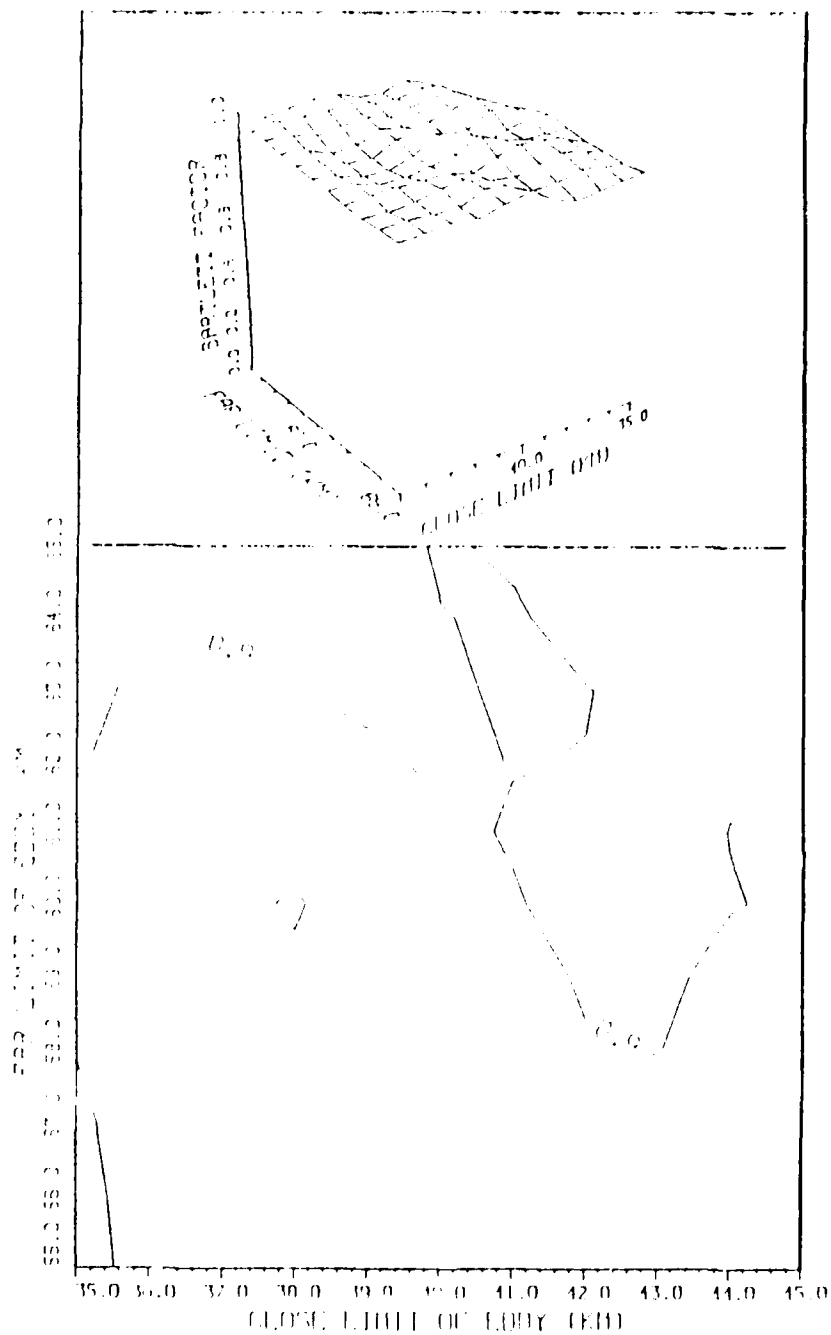
Figure 3.24   Eddy Localization.   Bartlett Estimator
Illustrating Condition of Strong Noise
Power and Moderate Noise Correlation,
$\sigma^2 = 10^{-15}$, $\rho = 1.7$
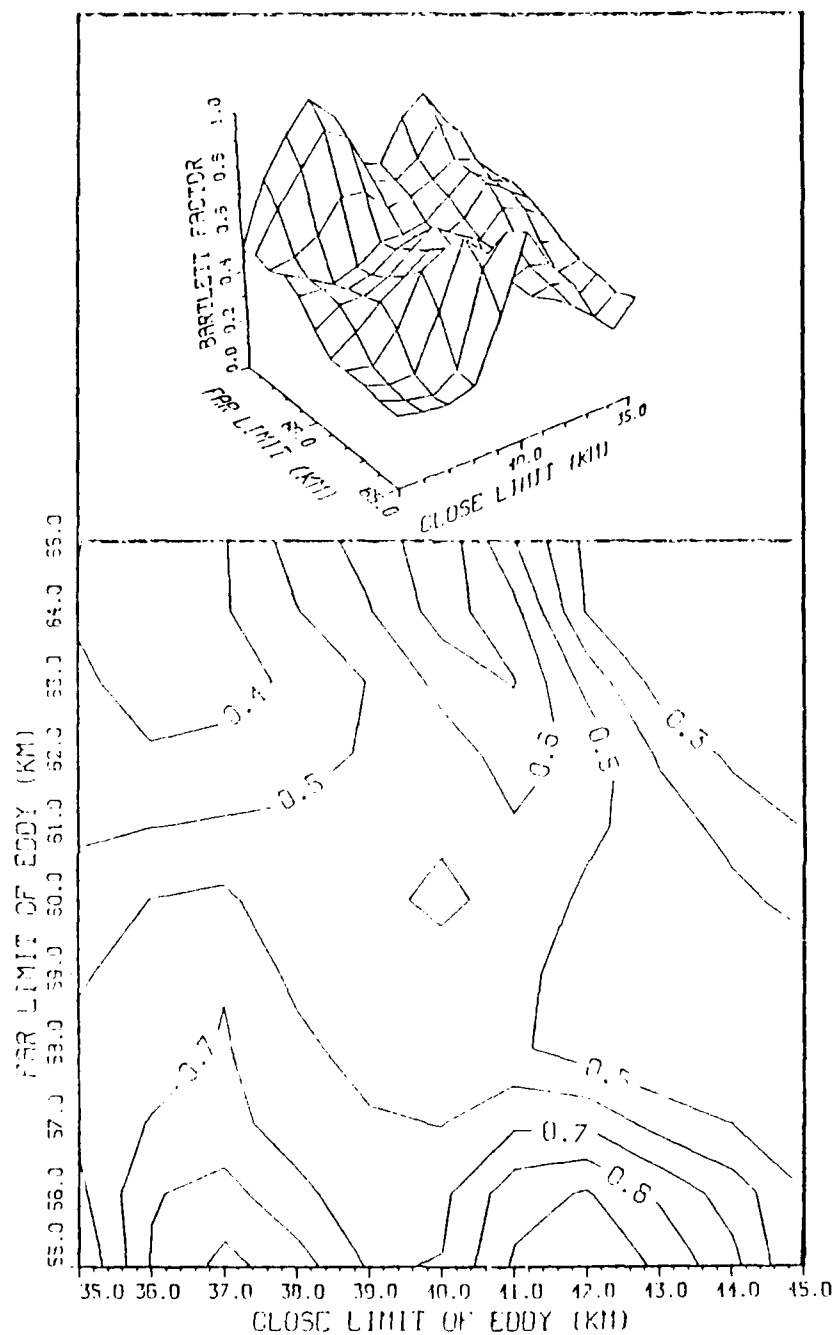
Figure 3.25   Eddy Localization. Bartlett Estimator
Illustrating Condition of Moderate Noise
Power and Strong Noise Correlation,
$\sigma^2 = 10^{-16}$, $R = 0.17$
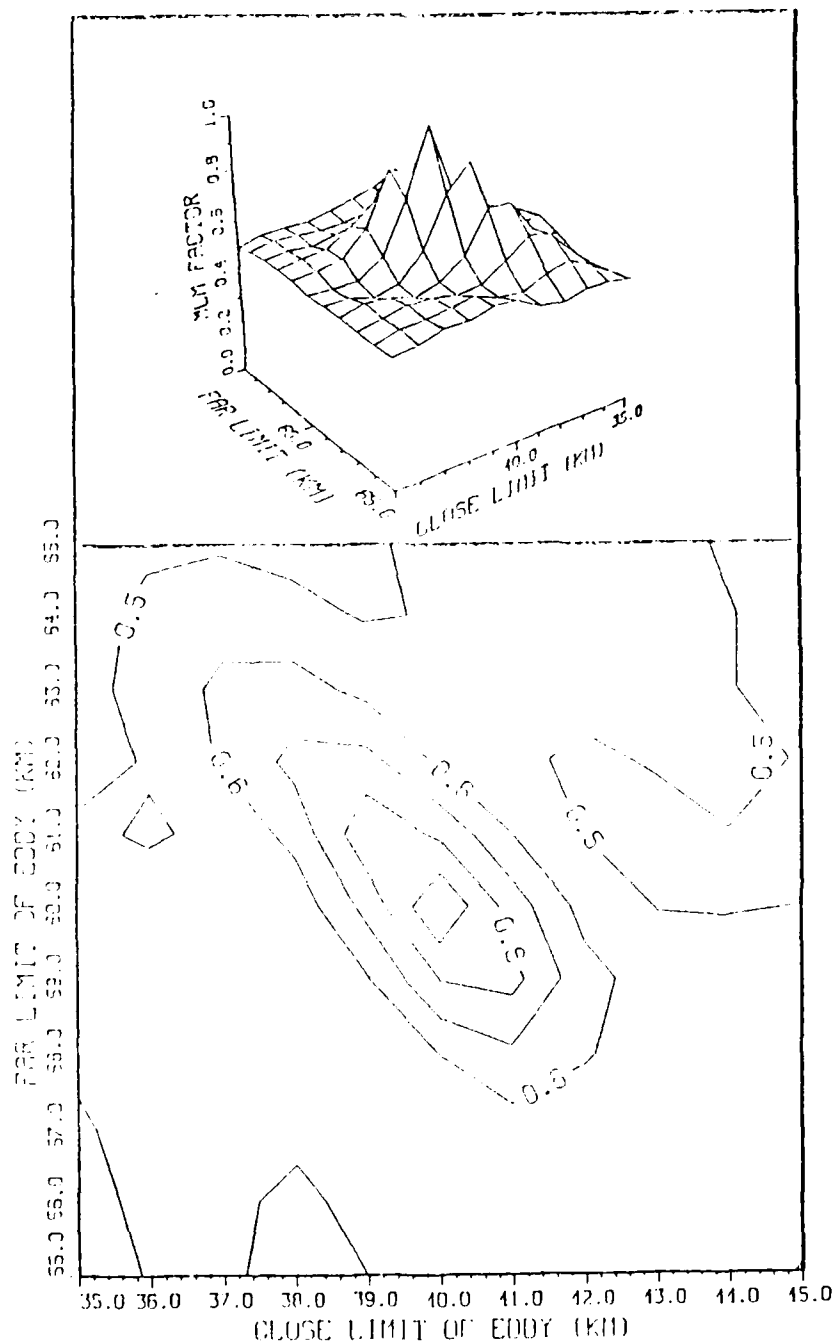
Figure 3.26   Eddy Localization. MLM Estimator Illustrating Condition of Moderate Noise Power and Moderate Noise Correlation, $\sigma^2 = 10^{-16}$, $\gamma = 1.7$
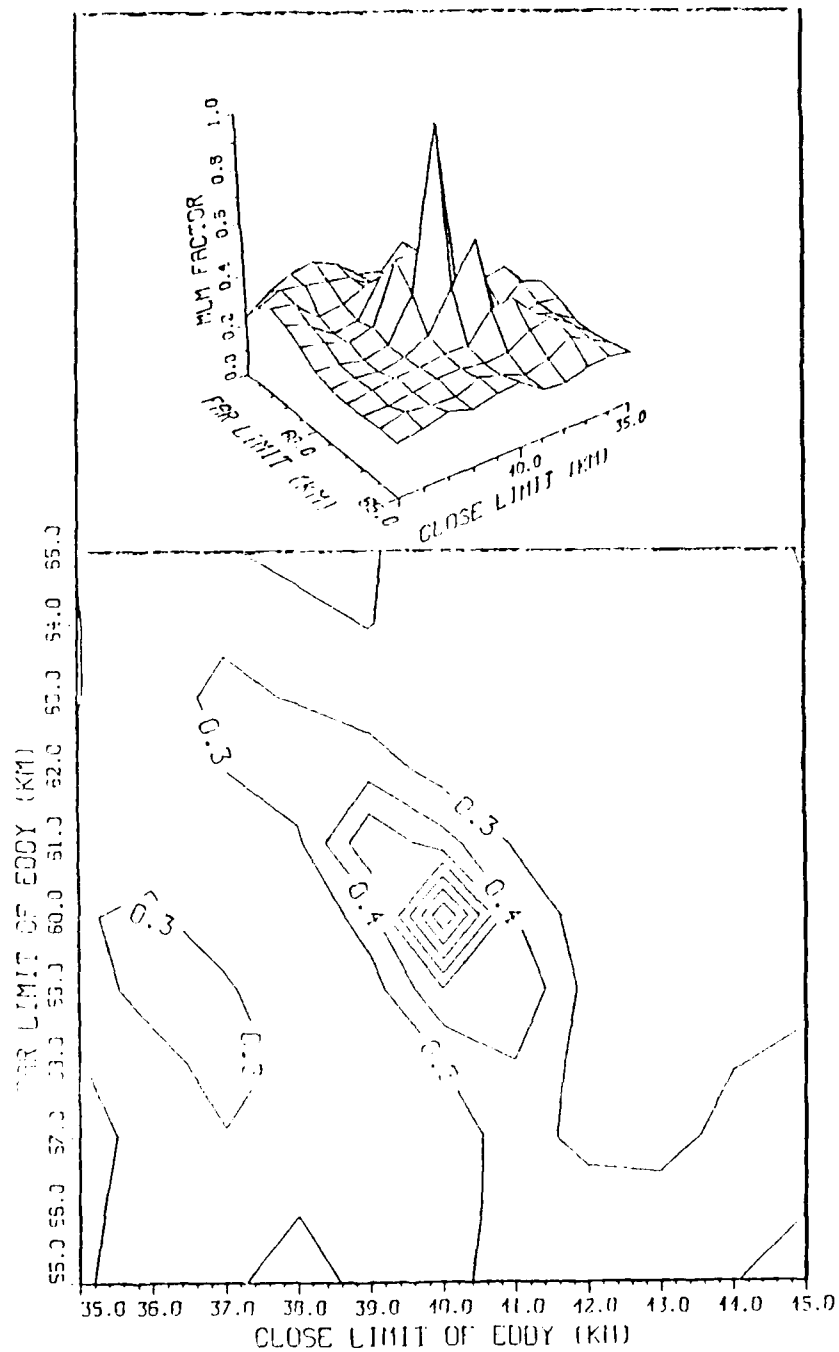
Figure 3.27   Eddy Localization.   MLM Estimator Illus-
            trating Condition of Moderate Noise
            Power and Strong Noise Correlation,
            $\sigma^2 = 10^{-16}$, $\Gamma = 0.17$
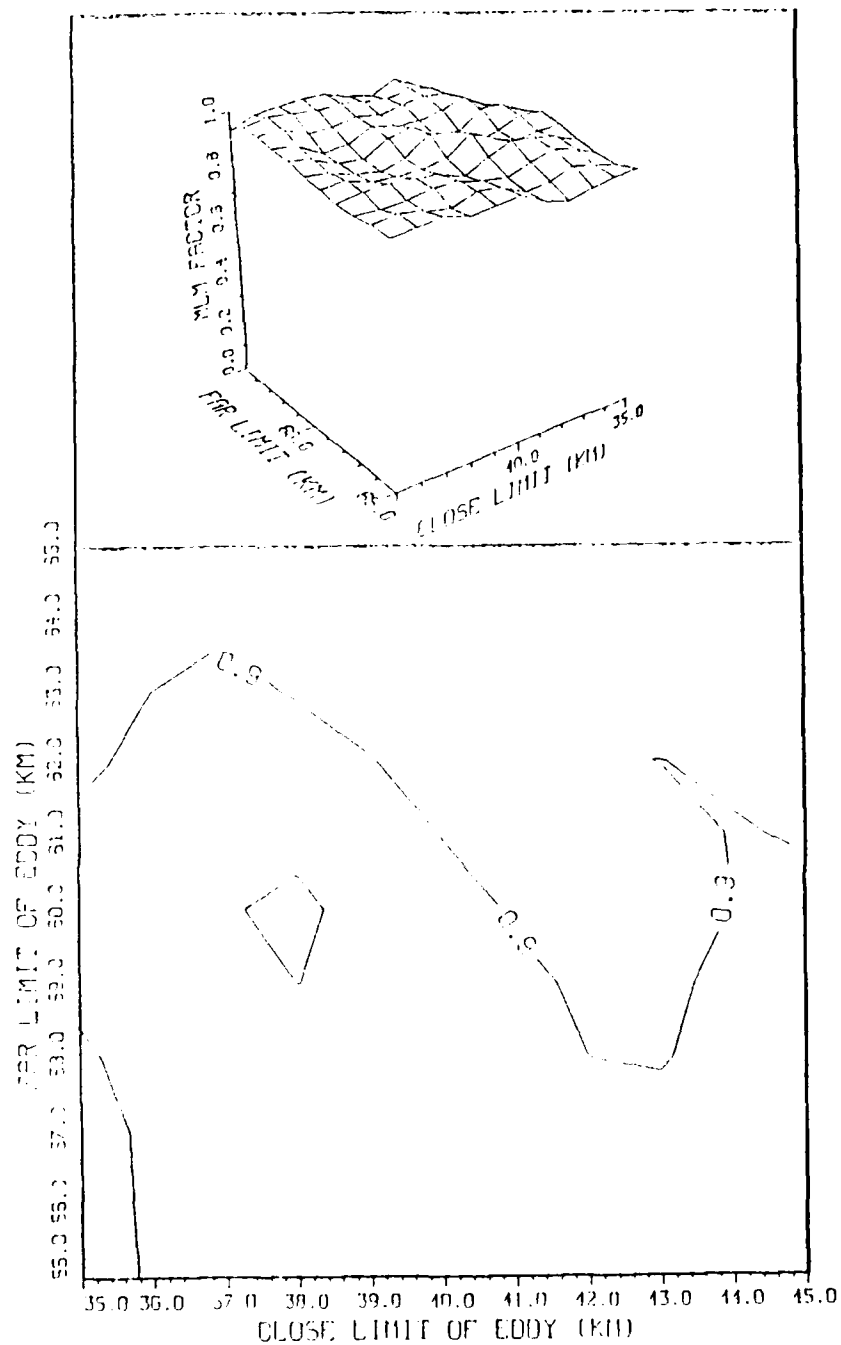
Figure 3.28 Eddy Localization. MLM Estimator Illus-
trating Condition of Strong Noise Power
and Moderate Noise Correlation, $\eta^2 = 10^{-15}$,
$F = 1.7$

IV. ANALYSIS OF THE SIMULATION

From the previous simulations, one sees that the performance of each of the estimators varies significantly under varying signal-to-noise ratios or source/receiver geometries or sound speed variations. For example, the center of gravity method was shown to be the best in locating the SOFAR axis and determining the surface sound speed. In contrast, this procedure was the least successful in the acoustic front localization problem. Therefore the efficiency of an estimator does not depend only on the type of ambient noise but also on the particular problem being solved. In order to continue focusing on a realistic problem, the eddy localization problem will be studied in greater detail. The condition of mismatching will be treated separately.

A. COMPARATIVE STUDY OF THE ESTIMATORS

1. Criterion

To facilitate comparison of the performance of the different methods, we will calculate the joint central moments of the different estimators. The joint central moment provides information on the spread of the detection factor about the mean. The smaller the moment, the better the estimate of the parameter of the ocean.

Using the definition of the central moment of a multiple random variable as defined by Peebles (1987):

$$\mu_{nk} = \int\int (x-\bar{X})^n (y-\bar{Y})^k f_{xy}(x,y) \, dx \, dy \qquad (4.1)$$

where:

$\bar{X}, \bar{Y}$ = means of the random variables X and Y,

f_{xy} = joint probability density function of X and Y,

n, k = orders of the central moment.

The spreading factor for the MLM method is defined as the second order central moment of the function MLM(x,y):

$$S = \int_x \int_y MLM(x,y) \, (x-40)^2 \, (y-60)^2 \, dx \, dy \qquad (4.2)$$

where x and y are the boundaries of the eddy we are looking for.

Since we are dealing with a discrete search among parameter values, this pseudo variance has the form:

$$S = \sum_{i=1}^{NR} \sum_{j=1}^{NR} MLM_{ij} \, (44+i-40)^2 \, (54+j-60)^2 \qquad (4.3)$$

where NF denotes the number of possible values of i and j.

Equation (4.3) indicates how the estimator spreads around the true frontal boundary values x = 40 and y = 60. It is a global measure of the estimator performance, not

just a measure of the main lobe width. A large value is associated with significant spreading which indicates a poor performance, even if the true position is actually found. The value of the spreading factor will be also large when the ambiguity surface has a large mean value and a small amplitude (case of significant noise). Analogous spreading factors may be defined for the Bucker and the Bartlett functions.

2. Efficiency of the Estimators

The spreading factor defined above has been computed for the different combinations of σ^2 and shown in Table 3.1. The results are presented in Table 4.1 for the Bucker, Bartlett and MLM methods. From this table it is possible to compare the efficiency of each technique in a variety of environments. The values of the correlation factor have been chosen to stay consistent with deep water measures. The range of noise powers, σ^2 produced signal-to-noise ratios between -67 dB and +21 dB.

In order to be consistent in comparing the spreading factor S of the three schemes, it is convenient to modify the expression for the Bucker detection factor as defined by Equation (2.4) by dividing it by its largest value among all the replicas. The maximum of this new function will always be one in all situations of noise, as the Bartlett and the MLM estimators.

TABLE 4.1

SPREADING FACTOR S OF THE BUCKER (NORMALIZED), BARTLETT AND MLM ESTIMATORS AS A FUNCTION OF σ^2 AND c

σ^2 \ c	0.57	1.00	1.70	2.00	2.20
10^{-19}	SNR=+13dB	SNR=+16dB	SNR=+20dB	SNR=+21dB	SNR=+21dB
	19,000	18,973	18,950	18,944	18,941
	25,924	25,902	25,884	25,880	25,877
	114	139	142	140	139
$5 \cdot 10^{-19}$	SNR=-1dB	SNR=+3dB	SNR=+6dB	SNR=+7dB	SNR=+7dB
	19,280	19,147	19,031	19,004	19,090
	26,471	26,364	26,272	26,250	26,239
	567	654	708	698	691
10^{-18}	SNR=-7dB	SNR=-3dB	SNR=0dB	SNR=+1dB	SNR=+1dB
	19,632	19,364	19,133	19,078	19,050
	27,149	26,935	26,754	26,710	26,688
	1,131	1,382	1,411	1,391	1,377
$5 \cdot 10^{-18}$	SNR=-21dB	SNR=-17dB	SNR=-14dB	SNR=-13DB	SNR=-12dB
	22,400	21,081	19,946	19,671	19,532
	32,328	31,320	30,463	30,258	30,153
	5,499	6,657	6,766	6,670	6,603
10^{-17}	SNR=-27dB	SNR=-23dB	SNR=-20dB	SNR=-19dB	SNR=-19dB
	25,773	23,188	20,950	20,407	20,131
	38,256	36,371	34,771	34,386	34,190
	10,630	12,732	12,883	12,687	12,570
10^{-16}	SNR=-47dB	SNR=-43dB	SNR=-39dB	SNR=-39dB	SNR=-38dB
	c	54,747	37,381	32,723	30,280
	c	85,126	78,315	76,655	75,805
	66,998	72,147	70,060	69,050	68,404
10^{-15}	SNR=-67dB	SNR=-63dB	SNR=-60dB	SNR=-59dB	SNR=-58dB
	c	c	c	c	c
	c	c	c	c	124,781
	c	c	c	c	124,584

Note 1: The signal-to-noise ratio is indicated for each entry of the table, followed by a triplet of numbers which represent, respectively, the Bucker (normalized), Bartlett and MLM spreading factors.

Note 2: The value c means that the estimator is unable to detect the true location of the eddy.

Table 4.1 provides a good illustration of the performance of the estimators under several conditions of noise power and correlation. Figures 4.1, 4.2 and 4.3 show logarithmic plots of the spreading factor S versus the noise power σ^2; each curve represents a value of the correlation parameter β. It is thus possible to determine the value of S for any pair of σ^2 and β. As is obvious from Table 4.1, the comparative performance of each method is mostly a function of the signal-to-noise ratio of the measure.

For SNR less than -50 dB all methods fail to detect the true location of the eddy. Nevertheless, we observe the case $\sigma^2 = 10^{-15}$ and $\beta = 2.2$, where the Bartlett and MLM estimators indicate two different maxima at one. Even in this case, the amplitude of the functions is so small that the spreading factor S is very large.

When the SNR is about -40 dB, the Bucker method is the most efficient estimator, albeit a weak one, as the spreading remains significant. The superiority of the scheme increases moreover when the correlation of the noise decreases.

For other SNR and correlation values, the MLM method is generally the most efficient. When the SNR = 0 dB or greater, the advantage of the MLM scheme is obvious with respect to the other two functions. One also notes that the MLM estimator is well adapted to resolving highly correlated noise situations; in such cases, simulations show that the

width of the main lobe becomes narrower but that the mean component of the surface increases.

B. MISMATCHING CASE

Mismatching occurs when a parameter used in simulation of the replica fields has been incorrectly estimated and is different from the one that created the true data. In the eddy localization problem, this defect may be introduced in several ways:

- a wrong measure of the source frequency,
- inaccurate estimation of the source or array position,
- inaccurate estimation of the source beamwidth,
- insufficient knowledge of the bottom loss characterization,
- oversimplification of the SSP.

This list is not exhaustive and one must keep in mind that perfect matching almost never exists due to the impossibility of any acoustic model to solve the true acoustic wave equation in the real ocean. Because mismatching prevents a close likelihood between the actual and replica fields. It can be thought of as an additional noise which the correlation matrix has not taken into account. Mismatching thus results in a degraded estimation of the total spatial correlation matrix KT. The next section studies in greater detail two cases where mismatching is created by a change in the bottom loss parameterization and where the borders of the eddy are

67

smoother than what we have used previously to simulate the real measured data.

1. Change in Bottom Loss Parameterization

All simulations were conducted with the assumption that the bottom was fully absorbing. We will now consider the bottom to be a perfectly rigid surface with total reflection and examine how this new treatment modifies the likelihood functions.

In the absence of noise the difference in phase at each receiver of the array for both the perfectly reflecting and fully absorbing bottom conditions is depicted in Figure 4.4. When the bottom is treated as a perfect reflector, perfect matching will not occur because all the replica fields are constructed based on the full absorption assumption.

Figures 4.5 and 4.6 show the result of a simulation using the MLM estimator with characteristics $^{-2} = 10^{-17}$ and $\vdots = 1.7$ to represent the situations of no mismatching and mismatching, respectively. When mismatching occurs, the amplitude of the peak decreases due to an increase in the mean value of the likelihood function. The secondary lobes also become larger. It is important to note that the degradation observed in Figure 4.6 does not imply that treating the bottom as a perfect reflector is less correct; it only means that the matching was done improperly; one

must therefore be consistent in modeling the environmental input variables.

2. Oversimplification of the Actual Eddy

The previously described eddy localization simulations were run with an excessive simplification of the true medium. The simulations assumed that there were no horizontal gradients of sound speed in and outside the eddy boundaries, i.e., the change of SSP occurred almost instantly at the borders of the eddy. In an attempt to be more realistic, the next simulation was conducted after adding four intermediate SSPs between the two previously utilized profiles (Figure 4.7). The first intermediate SSP was introduced 4 km before the border of the eddy and the next ones added every kilometer thereafter. Actual signal values were generated with this smoothed baroclinicity, and replica fields were computed as before with the simplistic three-profile model. Noise was omitted from this simulation in order to better appreciate the effect of this mismatching. Results for the Bucker method are presented in Figure 4.8. Comparing this plot with Figure 3.18 we see that the main peak decreases but localization of the eddy remains possible. The implication of this simulation is that identification (location) of strong frontal boundaries, such as the north wall of the Gulf Stream or ice edge fronts, could be fairly exact but weaker, open ocean mesoscale eddies may pose more of a difficult problem

69

(assuming the same number of profiles are used to estimate the replica fields).

The above examples suggest that in cases where the signal-to-noise ratio is quite low, it is possible for mismatching to hide the true location of the maximum and so possibly lead to a failure of the procedure. As often as possible, mismatching must be avoided by a comprehensive knowledge of the parameters used in the replica fields calculations.

C. COMMENTS ON THE PROCEDURE

As we were only interested in using matched field processing in acoustic tomography, many simplifications have been made to run the simulations. Although the procedure seems to be applicable and efficient in most cases, it is necessary to test its applicability to more complex problems.

1. Environment

It was assumed in all the simulations that only one or two parameters were unknown, for example, the surface sound speed or the eddy location. For actual oceanic situations, many more properties can be expected to vary in space and time. Extending this study to a heterogeneous medium is theoretically feasible but vastly increases the number of unknowns.

Modeling a shallow water environment has not been considered as a possible mechanism to speed up the

calculations even though matched field processing remains possible in this kind of environment. Several limitations are apparent. A better knowledge of the bottom structure is required. The ambient noise is moreover quite complex in coastal waters and its spatial correlation matrix would be difficult to model. As bottom interaction is important for estimator calculations (see the mismatching case), it is possible to consider the bottom loss as an unknown parameter and attempt to determine it through matched field processing. To examine this special case, the replica fields are generated using nine different bottom loss curves and one attempts to find the actual bottom loss curve. Figure 4.9 illustrates the different bottom loss curves that have been used to create the replica fields in shallow water (300 m). The maximum of the likelihood estimator occurs when the replica bottom corresponds to the actual loss. However, since the various curves are so similar in shape and because the bottom loss has only a weak to moderate effect on the transmission loss, the correct bottom loss curve is not sharply defined. This implies that a correct specification of bottom loss for a low loss bottom is not required; not so for a high loss bottom.

2. Model Consideration

a. Resolution

In the typical target location problem, the medium parameters are generally considered constant. It is

only necessary to run the PE model once to compute the pressure field at different distances. However, when the SSP becomes the unknown in the tomography problem, the PE model must be run for each replica. If we wish to find the correct shape of the SSP from 0 to 300 m in the seasonal thermocline with a resolution of 1 m, the model needs to be run 10^{300} times if the sound speed at each depth can have ten different values. This simple example illustrates the trade-off between resoluti ₁ and computer time. In the problem of eddy localization, where the limits of the perturbation were allowed to vary over 11 values, the PE model was run 121 times. For a determination of more than two unknowns, the basic theory of the estimators is still valid but the representation of the ambiguity surfaces becomes unachievable due to limitations in computer run time.

b. Noise Approximation

The correlation matrix of the ambient noise was modeled by a symmetric matrix decaying exponentially around the diagonal. This approximation is rather poor even in deep water, because the power of the noise is assumed to be the same at each hydrophone. A better simulation would have been to consider the matrix of a noise which is, like the signal, a so tion of the wave equation. Our matrix is symmetric even though the actual matrix of the complex noise

needs to be hermitian, because the cross-correlations are complex.

3. Correlation Matrix

If the spatial correlation matrix of the noise were known, it could be introduced in the replica fields and we could deal with it as with a noise-free problem.

In practice, it is not possible to separately compute the noise and the signal correlation matrices. The total matrix needs to be estimated from the noisy signal at the hydrophones. Several techniques are available, as for example the Fourier method recommended by Johnson (1982). As the matrix becomes only an estimate; we should expect a slight mismatching and then decreasing efficiency of the estimators.
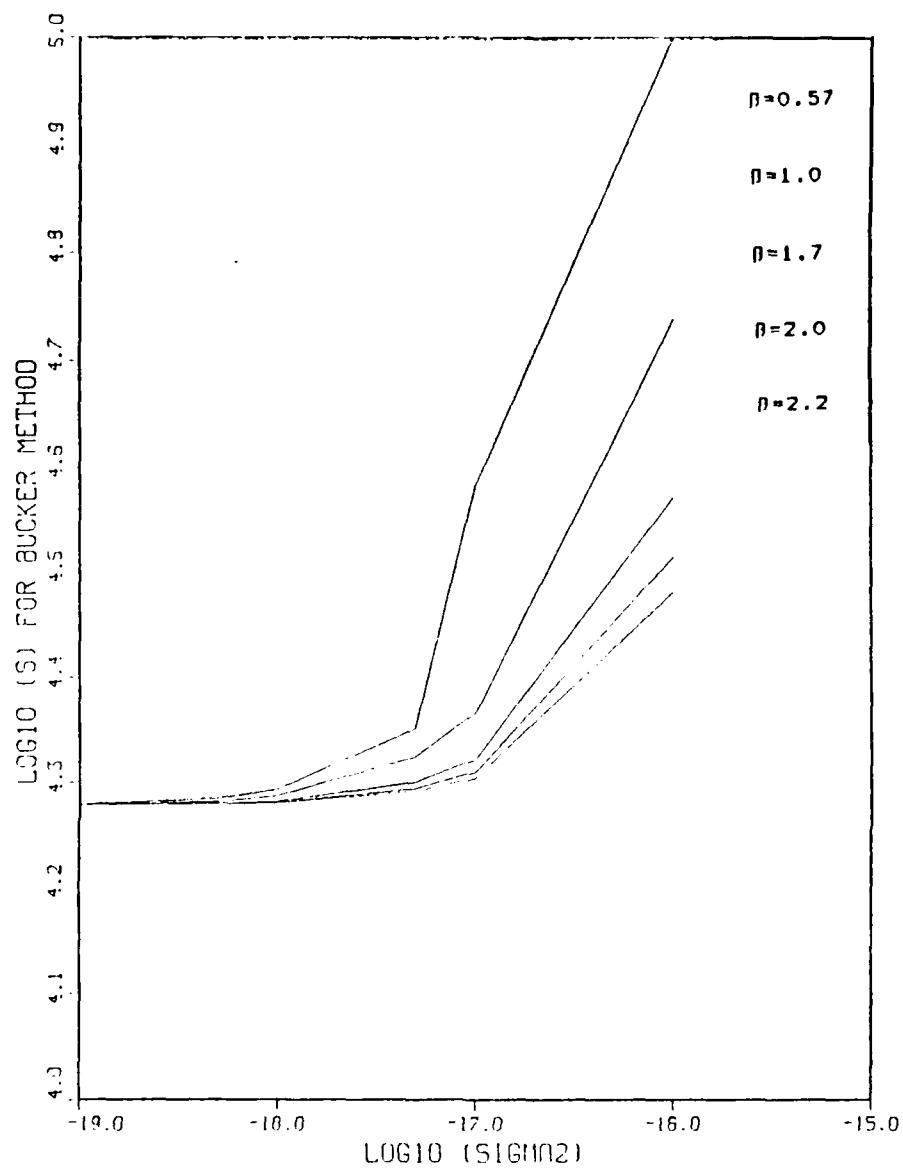
Figure 4.1   Eddy Localization.   Normalized Bucker
            Detection Factor.   Spreading Factor S as a
            Function of σ^2 for Various Conditions of
            Correlation, ρ

74
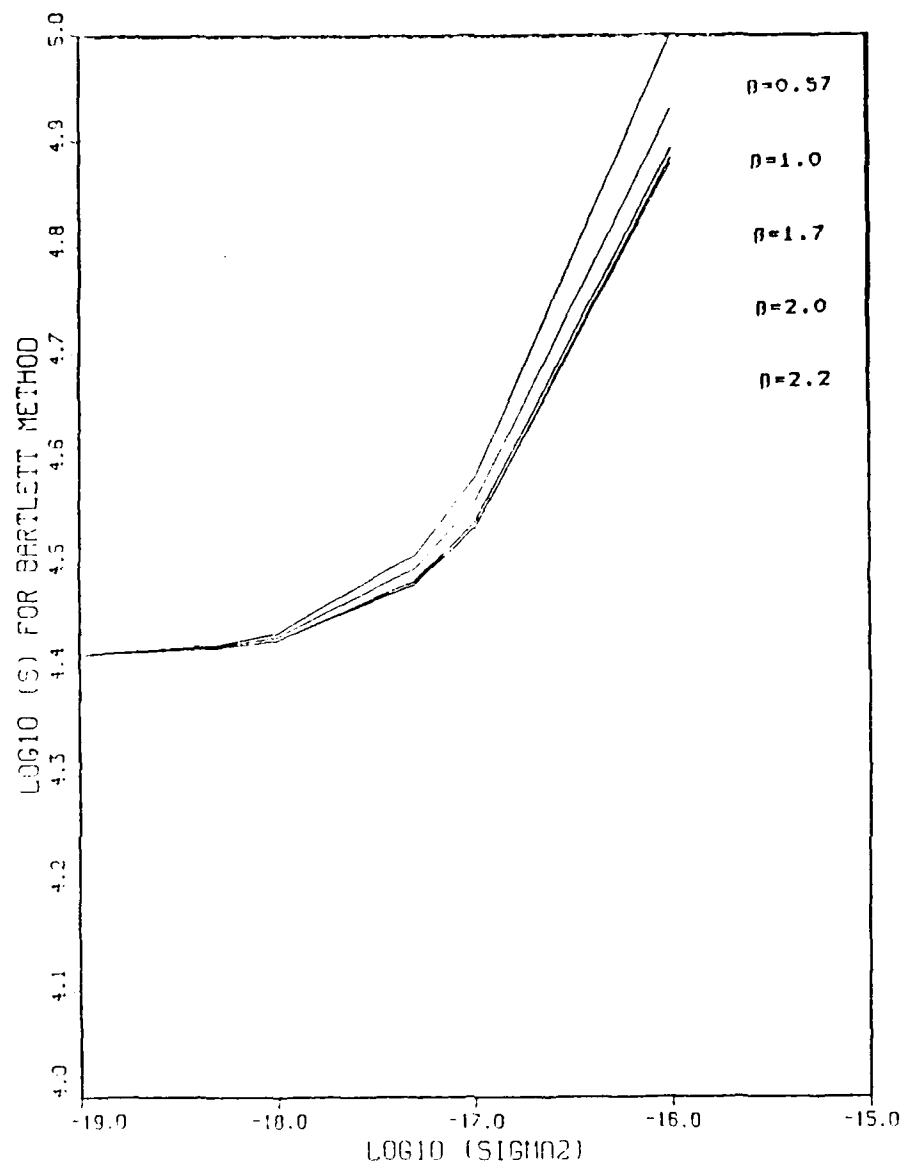
Figure 4.2   Eddy Localization.   Bartlett Estimator.
-        Spreading Factor S as a Function of σ^2 for
           Various Conditions of Correlation, ρ
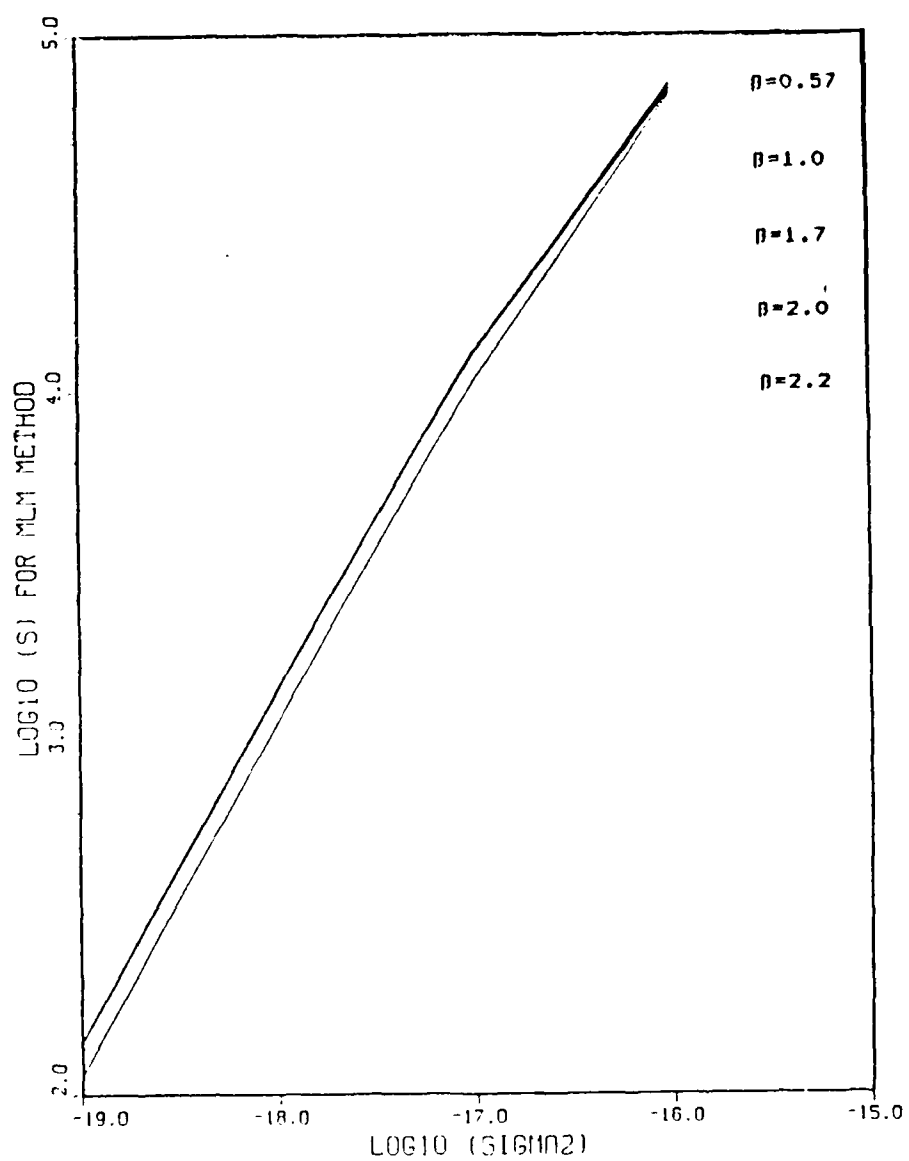
Figure 4.3 Eddy Localization, MLM Estimator.
          Spreading Factor S as a Function of σ^2
          for Various Conditions of Correlation, β

76
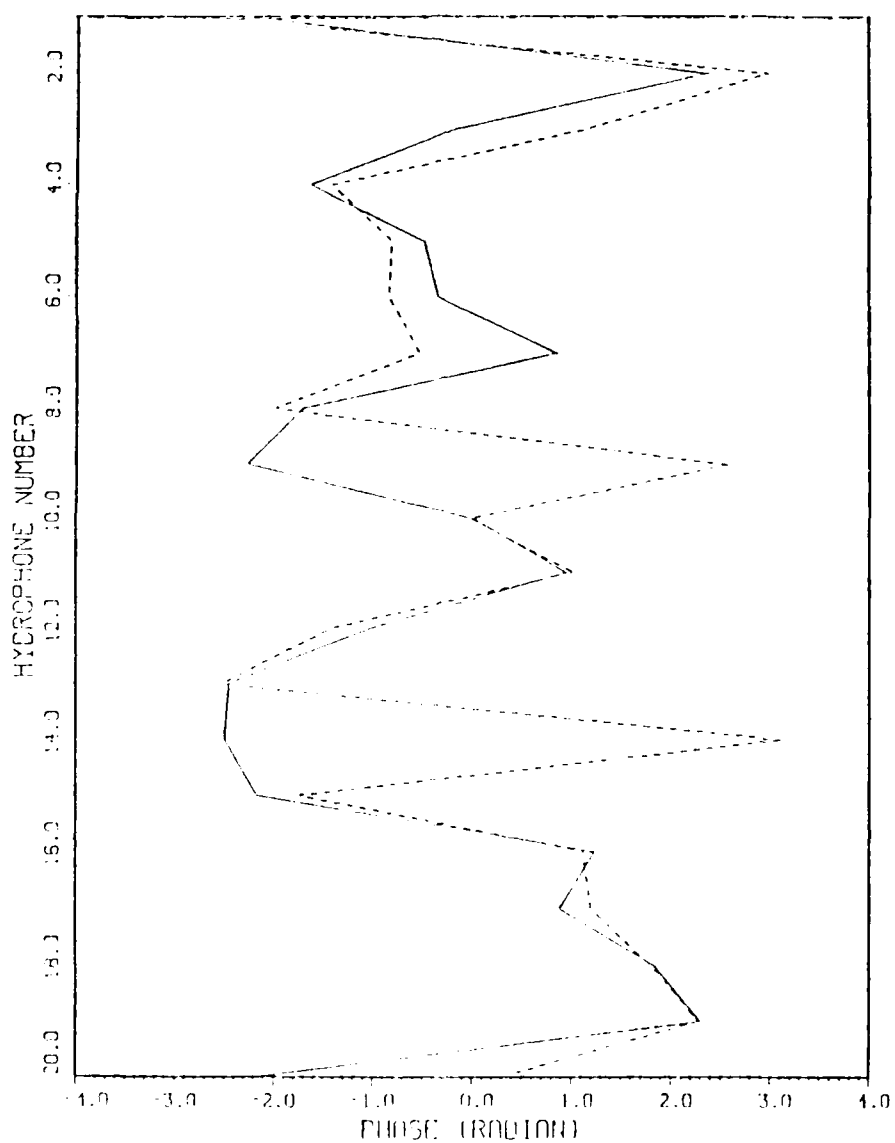
Figure 4.4 Phase of Complex Acoustic Pressure at the
Hydrophones for Fully Absorbing (___) and
Perfectly Reflecting (---) Bottom
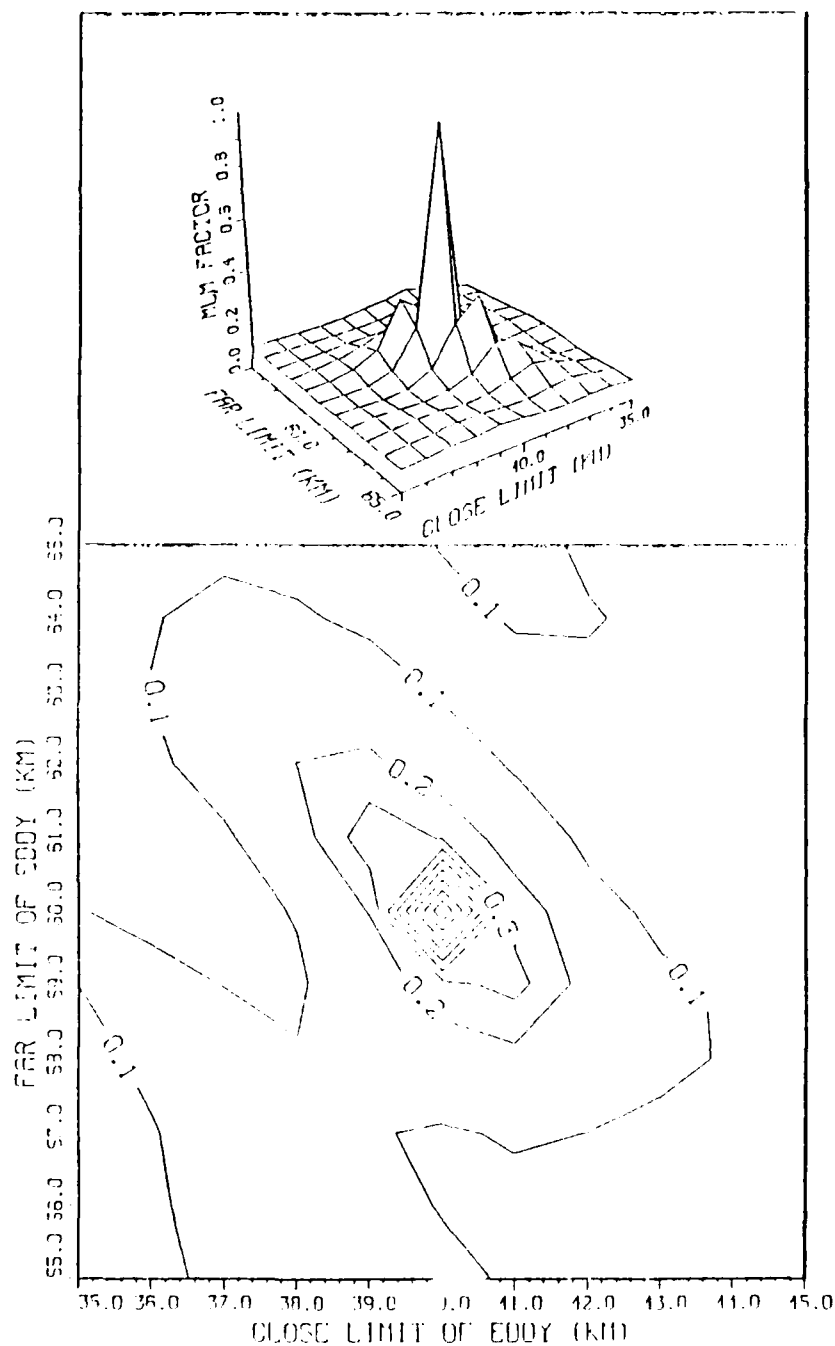
Figure 4.5 Eddy Localization. MLM Estimator,
$\sigma^2 = 10^{-17}$, $f = 1.7$. No Mismatching
(Bottom Treated as Fully Absorbing)
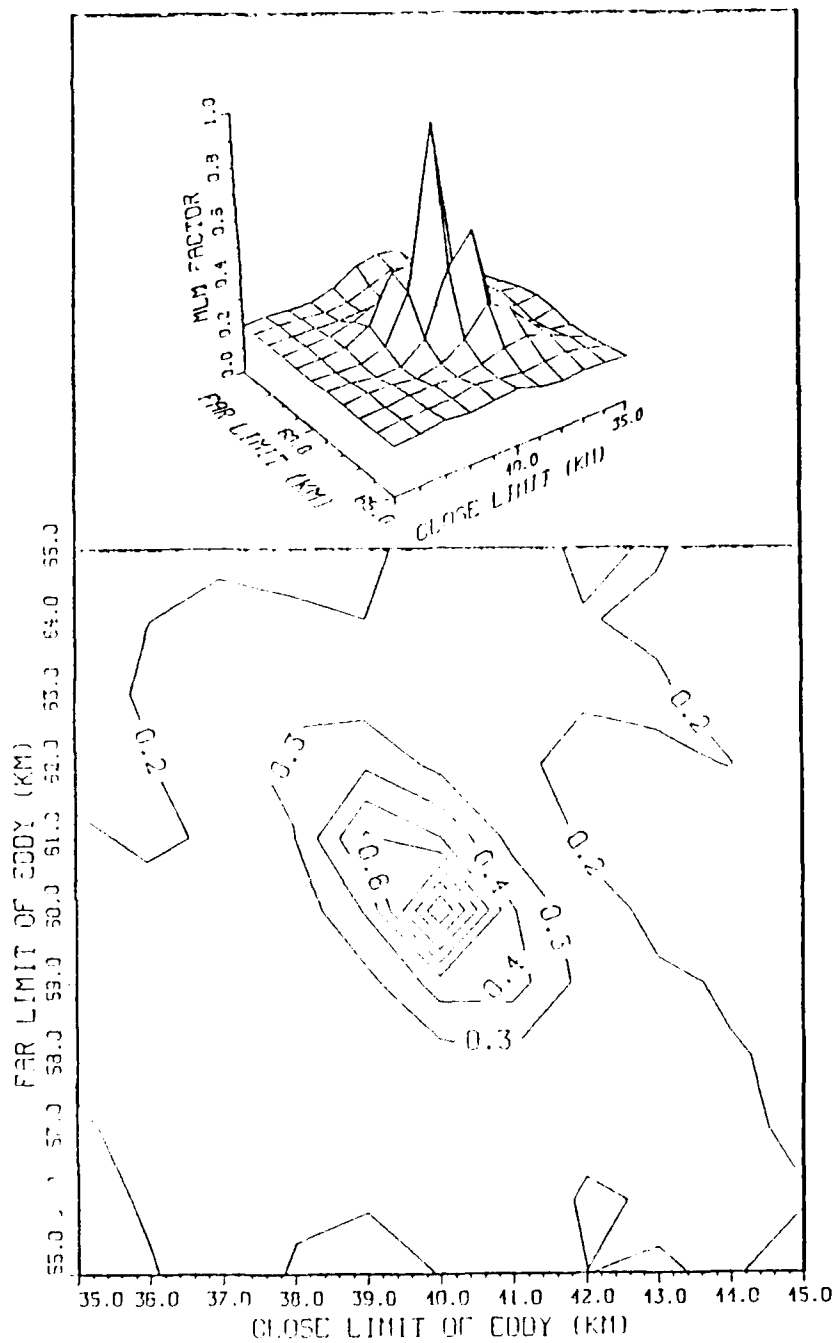
Figure 4.6 Eddy Localization. MLM Estimator,
$\sigma^2 = 10^{-17}$, $\rho \approx 1.7$. Mismatching
(Bottom Treated as Perfectly Reflecting)

79
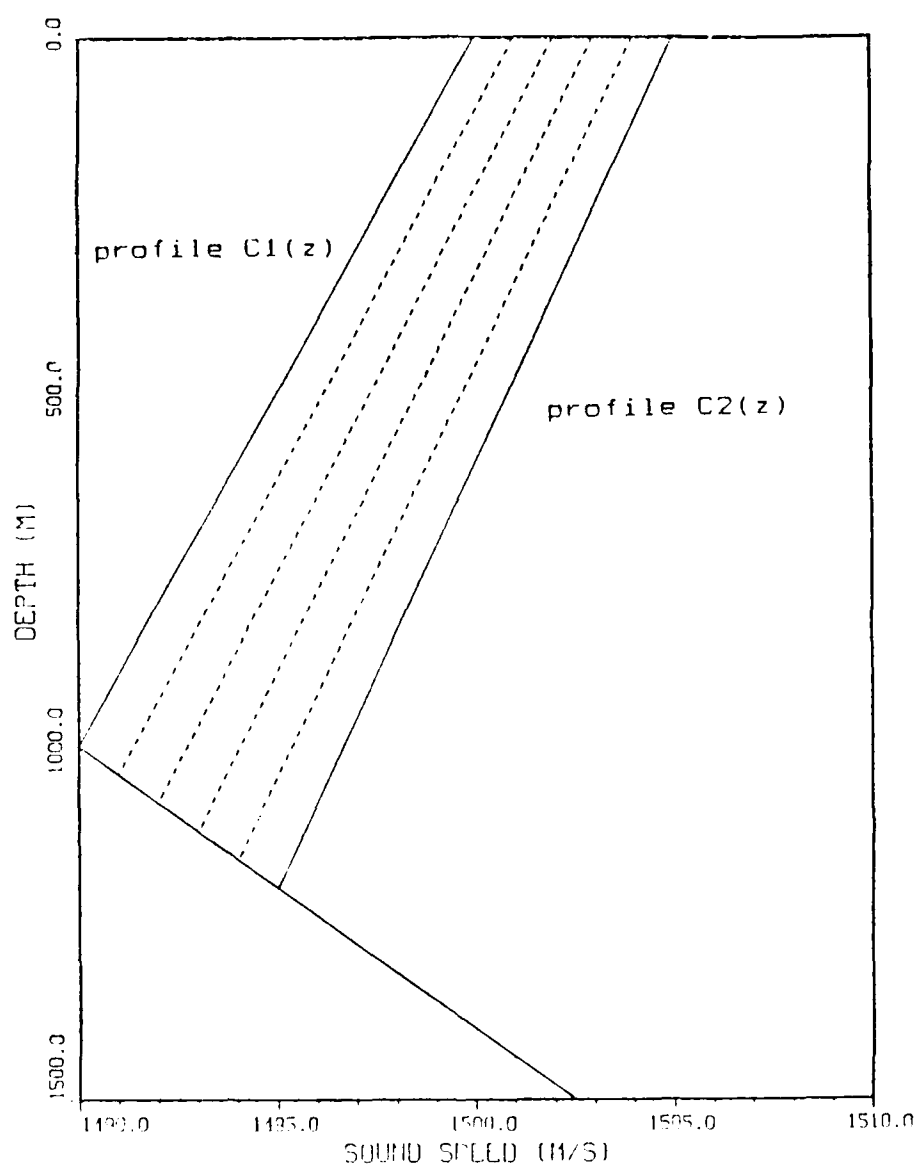
Figure 4.7   Intermediate SSPs (---) used for Transition
          -    from Open Ocean SSP (cl(z)) to the Eddy SSP
               (c2(z))

80
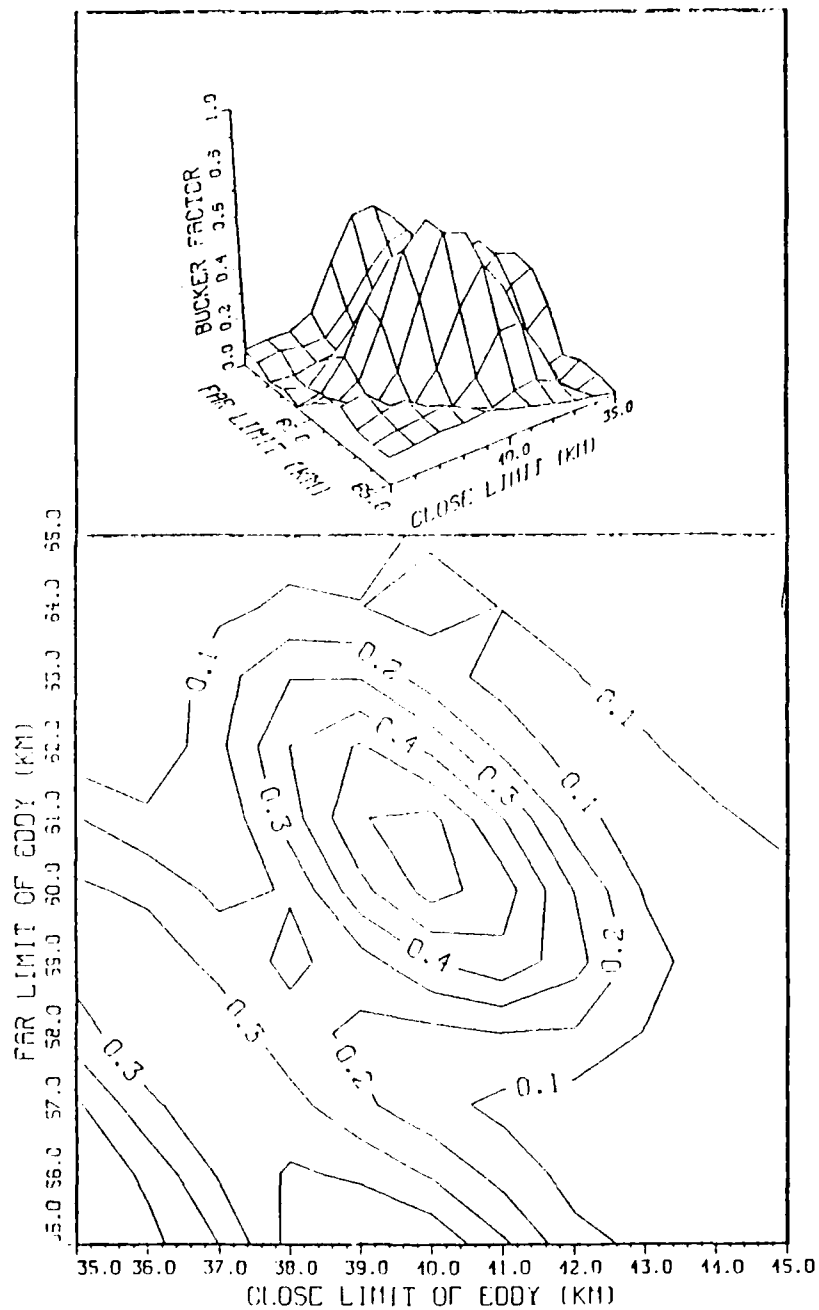
Figure 4.8 Eddy Localization. Bucker Detection Factor.
            Mismatching Due to an Excessive Simplifica-
            tion of Horizontal Sound Speed Gradients
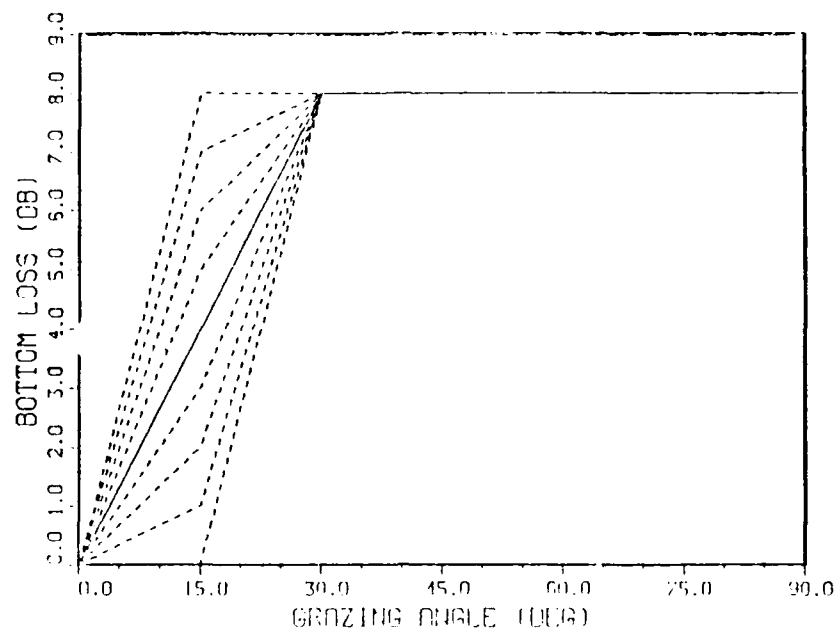
(a)
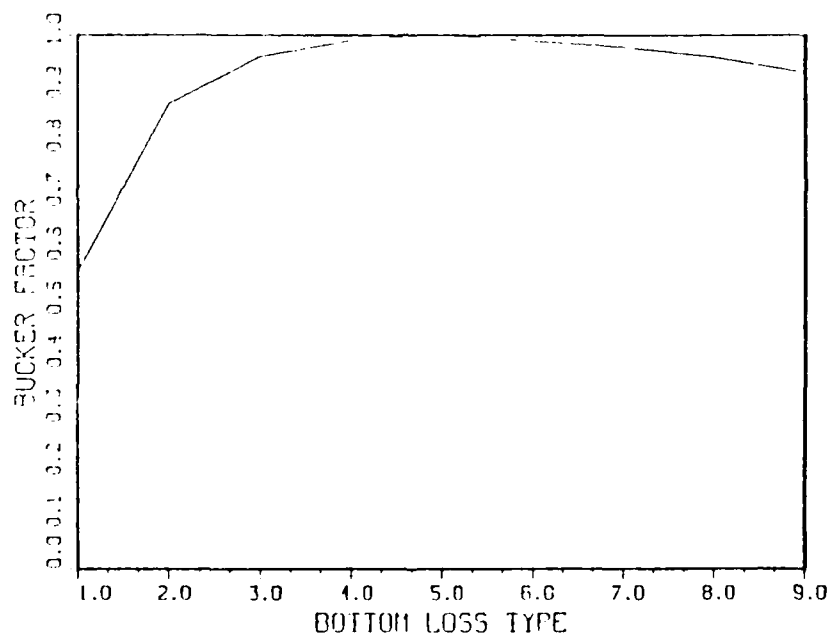
(b)

Figure 4.9   Bottom Loss Determination.   Bucker Detection
        Factor.   Replica Bottom Loss Curves (a).
        Estimation of Bottom Loss Curve (b)

V. CONCLUSION

Matched field processing has been shown to be an efficient way to solve the inverse problem in ocean acoustic tomography when the ocean can be characterized by a few parameters. The estimators which have been used (Bucker, Bartlett, Maximum Likelihood, etc.) were generally robust enough to find the actual sound speed field of the ocean under usual conditions of noise power and noise correlation.

A. SUMMARY OF THE RESULTS

For noise-free conditions or high signal-to-noise ratios (SNR), all the estimators are able to correctly determine the actual unknown parameter of the medium. The Bucker detection factor was shown to be the best function when the SNR was moderate.

The efficiency of the various estimators, illustrated by their spreading about the true value, decreased in cases of low SNR introduced by a large power or a high spatial correlation of the noise. The Maximum Likelihood method was shown to be the best scheme when the ambient noise was highly correlated because its spreading was less sensitive to the degree of spatial correlation than the other estimators.

The effect of mismatching, when introduced in the simulations, generated a decrease in the efficiency of the

83

methods.   Analysis of several degrees of mismatching indicated that unambiguous results can be expected from matched field processing provided that the parameterization of the medium is exact enough to generate consistent replica pressure fields.

B.   WEAKNESS OF THE SIMULATION

In order to deal with reasonable computer times, only the cases of one or two unknown parameters were studied. For the same reason, the actual acoustic pressure field was compared with only a few replica fields.   This limitation leads to moderate resolution in the results which could easily be improved by the generation of more replica fields.

The weakness in modeling the noise field has already been emphasized in Chapter III.A.   Further simulations should be done with a noise correlation matrix, KN, that has actually been obtained from measurements at sea.   Further work using a more realistic parameterization of the ocean should be done, e.g., with empirical orthogonal functions (EOF) and using the technique to estimate EOF coefficients.

FORTRAN 77 PROGRAM USED IN THE SIMULATION

```
      PROGRAM ESTIMA
C     ACOUSTIC TOMOGRAPHY USING MATCHED FIELD PROCESSING
C
C     THIS PROGRAM DRAWS THREE KINDS OF DETECTION FACTOR IN 3D
C     IT COMPARES BUCKER,BARTLETT AND MLM METHODS
C
C     THE NOISE IS INTRODUCED BY ITS CORRELATION MATRIX
C
C     THE NOISE MATRIX IS PROPORTIONAL TO IDENTITY MATRIX IN CASE OF
C     UNCORRELATED NOISE BUT IS IN GENERAL HERMITIAN MATRIX
C
C     THE EXACT(OR MEASURED) PHASES AND MAGNITUDES ARE READ IN THE
C     FILE EXACT DATA
C     THE COMPUTED PARAMETERS ARE READ ON THE FILE NEAR DATA
C
C     THE MODEL ALLOWS A MAXIMUM OF 20 RECEIVERS DUE TO THE USE OF THE
C     PARABOLIC EQUATION FROM THE EARG PACKAGE
C
C     KS IS THE COMPLEX MATRIX OF MEASURED PARAMETERS
C     A IS THE MATRIX OF GUESSED PARAMETERS WE WANT TO MATCH
C     NR IS THE NUMBER OF RECEIVERS(MAXIMUM 20)
C     NF IS THE COMMON NUMBER OF POSSIBLE VALUES FOR 2 UNKNOWNS
C     THE NUMBER OF FIELDS WE MATCH IS ACTUALLY NF*NF
C
C
      REAL PPHASE(20),PMAGNI(20),X(11),Y(11),DF(11,11),DFCONT(11,11)
      REAL BART(11,11),FMLM(11,11),MCONT(11,11),BCONT(11,11)
      COMPLEX A(20,20),KS(20,20),CDF(11,11),KT(20,20)
      COMPLEX W(20),CSUM,DETERM
      REAL KN(20,20),NORM
C     99 DEFINES THE FILE OF MEASURED(EXACT) DATA
C     98 DEFINES THE FILE OF DATA WE WANT TO MATCH
      NR=20
      NF=11
C     READ THE MEASURED VALUES IN FILE EXACT DATA
      DO 1  I=1,NR
        READ(99,600) PMAGNI(I),PPHASE(I)
1     CONTINUE
600   FORMAT(   E11.4,2X,F7.4)
C
C
C     COMPUTE THE ELEMENTS OF MATRIX KS
999   DO  2 J=1,NR
        DO 3  K=1,NR
          KS(J,K)=PMAGNI(J)*PMAGNI(K)*EXP(CMPLX(0.,PPHASE(J)-
     *      PPHASE(K)))
3       CONTINUE
2     CONTINUE
```

```
****************************************************************
C       DEFINE THE CORRELATION MATRIX KN OF THE CORRELATED NOISE
        PRINT*,' VALUE OF SIGMA2 ?'
        READ*,SIGMA2
        PRINT*,' VALUE OF BETA ?'
        READ*,BETA
        DO 4  J=1,NR
          DO 5  I=1,NR
            KN(I,J)=SIGMA2*EXP(-BETA*ABS(I-J))
5         CONTINUE
4       CONTINUE
****************************************************************
C
C       COMPUTE THE TOTAL COVARIANCE MATRIX INCLUDING THE NOISE
C       BY ADDING THE NOISE AND THE SIGNAL CORRELATION MATRICES
        DO  6 J=1,NR
          DO  7 I=1,NR
        KT(I,J)=KS(I,J)+KN(I,J)
7         CONTINUE
6       CONTINUE
C
C
C       BEGINNING OF MAIN LOOP FOR THE NF RUNS

        DO 101  INDEX=1,NF
        DO 100 JNDEX=1,NF
C       READ PARAMETERS OF EXPECTED FIELD IN FILE NEAR DATA
          DO  8 I=1,NR
            READ(98,600) PMAGNI(I),PPHASE(I)
8         CONTINUE
C
C       COMPUTE ELEMENTS OF MATRIX A
        DO 9  J=1,NR
          DO 10 K=1,NR
            A(J,K)=PMAGNI(J)*PMAGNI(K)*EXP(CMPLX(0., PPHASE(J)-
     *         PPHASE(K)))
10        CONTINUE
9       CONTINUE
CCCCCCCCCCCCCCCCCCCCCCCCCCCCCCCCCCC
C       BUCKER DETECTION FACTOR C
CCCCCCCCCCCCCCCCCCCCCCCCCCCCCCCCCCC
        CDF(INDEX,JNDEX)=CMPLX(0.,0.)
        DO 11 J=1,NR
          DO 12 K=1,NR
            IF(K.NE.J) CDF(INDEX,JNDEX)=CDF(INDEX,JNDEX)+
     *      A(J,K)*CONJG(KT(J,K))
12        CONTINUE
11      CONTINUE
C
C       CDF(--,--) IS ACTUALLY REAL DUE TO PROPERTY OF MATRICES
C       A AND KT HENCE WE KEEP ONLY THE REAL PART OF IT
        DF(INDEX,JNDEX)=REAL(CDF(INDEX,JNDEX))
C
C       NORMALIZE THE DF FACTOR
        FACTOR=0.
        FACT=0.
        DO 13  J=1,NR
          DO 14 K=1,NR
            IF(K.NE.J)FACTOR=FACTOR+A(J,K)*CONJG(A(J,K))
            IF(K.NE.J)FACT=FACT+KT(J,K)*CONJG(KT(J,K))
14        CONTINUE
13      CONTINUE
```

```
      FACTOR=SQRT(FACTOR)
      FACT=SQRT(FACT)
      DF(INDEX,JNDEX)=DF(INDEX,JNDEX)/FACT/FACTOR
      DF(INDEX,JNDEX)=ABS(DF(INDEX,JNDEX))
C
100   CONTINUE
101   CONTINUE
C
C     NORMALIZE BY THE LARGEST VALUE
      BMAX=0.
      DO 67 I=1,NF
         DO 68 J=1,NF
            IF(DF(I,J).GE.BMAX) BMAX=DF(I,J)
68       CONTINUE
67    CONTINUE
C
      DO 69 I=1,NF
         DO 70 J=1,NF
            DF(I,J)=DF(I,J)/BMAX
70       CONTINUE
69    CONTINUE

C
C     DISSPLAY THE MATRIX  OF NORMALIZED DETECTION FACTOR
      PRINT*,  BUCKER FACTOR MATRIX
      DO 15  I=1,NF
         WRITE(6,777)(DF(I,J),J=1,NF)
777      FORMAT(11(2X,F4.2))
15    CONTINUE
C
CCCCCCCCCCCCCCCCCCCCCCCCCCCCC
C      BARTLETT ESTIMATOR C
CCCCCCCCCCCCCCCCCCCCCCCCCCCCC
      REWIND 98

C     BEGINNING OF MAIN LOOP FOR THE NF RUNS
      DO 201  INDEX=1,NF
      DO 200 JNDEX=1,NF
C
C     READ PARAMETERS OF REPLICA FIELD
      DO 50 I=1,NR
         READ(98,600) PMAGNI(I),PPHASE(I)
50    CONTINUE
C
C     DETERMINE THE NORMALIZED COMPLEX VECTOR W
      NORM=0.
      DO 16 I=1,NR
         NORM=NORM+PMAGNI(I)**2
16    CONTINUE
      NORM=SQRT(NORM)
C
      DO 17 I=1,NR
         W(I)=(1./NORM)*PMAGNI(I)* EXP(CMPLX(0.,PPHASE(I)))
17    CONTINUE
C
C     COMPUTE THE BARTLETT FACTOR
      CSUM=(0.,0.)
      DO 18 I=1,NR
         DO 19 J=1,NR
            CSUM=CSUM+CONJG(W(I))*KT(I,J)*W(J)
19       CONTINUE
18    CONTINUE
      BART(INDEX,JNDEX)=REAL(CSUM)
```

```
C
200     CONTINUE
201     CONTINUE
C
C       NORMALIZATION BY THE HIGHEST VALUE
        BARMAX=0.
        DO 20  I=1,NF
           DO 21   J=1,NF
              IF(BART(I,J).GE.BARMAX) BARMAX=BART(I,J)
21         CONTINUE
20      CONTINUE
C
        DO 22  I=1,NF
           DO 23  J=1,NF
              BART(I,J)=BART(I,J)/BARMAX
23         CONTINUE
22      CONTINUE
C
C       DISSPLAY THE MATRIX  OF NORMALIZED DETECTION FACTOR
        PRINT*,  BARTLETT FACTORS MATRIX'
        DO 24  I=1,NF
           WRITE(6,777)(BART(I,J),J=1,NF)
24      CONTINUE
C
CCCCCCCCCCCCCCCCCCCCCCCC
C       MLM ESTIMATOR C
CCCCCCCCCCCCCCCCCCCCCCCC
        REWIND 98
C
C       INVERT THE CORRELATION MATRIX KT
        CALL CMTRIN(NR,KT,NR,DETERM)
C
C       BEGINNING OF MAIN LOOP FOR THE NF RUNS
        DO 301  INDEX=1,NF
        DO 300 JNDEX=1,NF
C
C       READ PARAMETERS OF REPLICA FIELD
        DO 51 I=1,NR
           READ(98,600) PMAGNI(I),PPHASE(I)
51      CONTINUE
C
C       DETERMINE THE NORMALIZED COMPLEX VECTOR W
        NORM=0.
        DO 26 I=1,NR
           NORM=NORM+PMAGNI(I)**2
26      CONTINUE
        NORM=SQRT(NORM)
C
        DO 27 I=1,NR
           W(I)=(1./NORM)*PMAGNI(I)* EXP(CMPLX(0.,PPHASE(I)))
27      CONTINUE
C
C       COMPUTE THE MLM FACTOR
        CSUM=(0.,0.)
        DO 28 I=1,NR
           DO 29 J=1,NR
              CSUM=CSUM+CONJG(W(I))*KT(I,J)*W(J)
29         CONTINUE
28      CONTINUE
        FMLM(INDEX,JNDEX)=REAL(1./CSUM)
C
300     CONTINUE
301     CONTINUE
```

```fortran
C
C       NORMALIZATION BY THE HIGHEST VALUE
        FMLMAX=0.
        DO 30   I=1,NF
          DO 31   J=1,NF
            IF(FMLM(I,J).GE.FMLMAX) FMLMAX=FMLM(I,J)
31        CONTINUE
30      CONTINUE
C
        DO 32   I=1,NF
          DO 33   J=1,NF
            FMLM(I,J)=FMLM(I,J)/FMLMAX
33        CONTINUE
32      CONTINUE
C
C       DISSPLAY THE MATRIX  OF NORMALIZED DETECTION FACTOR
        PRINT*,' MLM FACTORS MATRIX'
        DO 34   I=1,NF
          WRITE(6,777)(FMLM(I,J),J=1,NF)
34      CONTINUE
C
C
CCCCCCCCCCCCCCCCCCCCCCCCCCCCCCCCCCCCCCCCCCCCCCCCCCCCCCCCCCC
C       COMPUTE THE SPREADING FACTOR OF THE ESTIMATORS C
CCCCCCCCCCCCCCCCCCCCCCCCCCCCCCCCCCCCCCCCCCCCCCCCCCCCCCCCCCC
        WDF=0.
        WBART=0.
        WFMLM=0.
        DO 650 I=1,NF
          DO 651 J=1,NF
            WDF=WDF+DF(I,J)*(44.+I-40.)**2*(54+J-60)**2
            WBART=WBART+BART(I,J)*(44.+I-40.)**2*(54+J-60)**2
            WFMLM=WFMLM+FMLM(I,J)*(44.+I-40.)**2*(54.+J-60.)**2
651       CONTINUE
650     CONTINUE
C
C
        PRINT*,' WDF= ',WDF
        PRINT*,' WBART= ',WBART
        PRINT*,' WFMLM= ',WFMLM
C
C
        END
```

LIST OF REFERENCES

Baggeroer, A.B., Kuperman, W.A., and Schmidt, H., "Matchfield Processing: Source Localization in Correlated Noise as an Optimum Parameter Estimation Problem," The Journal of the Acoustical Society of America, Vol. 83, pp. 571-587, February 1988.

Bucker, H.P., "Use of Calculated Sound Fields and Matched-Field Detection to Locate Sound Sources in Shallow Water," The Journal of the Acoustical Society of America, Vol. 59, pp. 368-373, February 1976.

Coppens, A.B., An Introduction to the Parabolic Equation for Acoustic Propagation, Naval Postgraduate School Report 61-83-002, November 1982.

Cox, H., "Spatial Correlation in Arbitrary Noise Fields with Application to Ambient Sea Noise," The Journal of the Acoustical Society of America, Vol. 54, pp. 1289-1301, April 1973.

Heitmeyer, R.M., Fizell, R.G., and Moseley, W.B., Full Field Ambiguity Function Processing in a Complex Shallow-Water Environment, Naval Research Laboratory Report 8868, 31 December 1984.

Howe, B.M., Ocean Acoustic Tomography: Mesoscale Velocity, Ph.D. Dissertation, Scripps Institution of Oceanography, San Diego, California, 1986.

Johnson, D.H., "The Application of Spectral Estimation Methods to Bearing Estimation Problems," IEEE (JOE), Vol. 70, pp. 1018-1028, 1982.

Kay, S.M., Modern Spectral Estimation. Theory and Application, Prentice Hall, Englewood Cliffs, New Jersey, 1988.

Munk, W., and Wunsch, C., "Ocean Acoustic Tomography: A Scheme for Large Scale Monitoring," Deep-Sea Research, Vol. 26A, pp. 123-161, July 1978.

Peebles, P.Z., Probability, Random Variable, and Random Signal Principles, p. 120, McGraw-Hill Book Co., San Francisco, California, 1987.

Porter, M.B., Dicus, R.L., and Fizell, R.G., "Simulation of Matched Field Processing in a Deep Water Pacific Environment," IEEE (JOE), Vol. 01, pp. 173-181, January 1987.

Schmidt, R.O., _A Signal Subspace Approach to Multiple Emitter Location and Spectral Estimation_, Ph.D. Dissertation, Stanford University, November 1981.

Urick, R.J., _Ambient Noise in the Sea_, pp. 6-11, Peninsula Publishing, Co., Los Altos, California, 1984.

Ziomek, J.L., _Underwater Acoustics--A Linear Theory Approach_, pp. 122-123, Academic Press, Inc., Orlando, Florida, 1985.

BIBLIOGRAPHY

Romm, J.J., _Application of Normal Mode Analysis to Ocean Acoustic Tomography_, Ph.D. Dissertation, Massachusetts Institute of Technology, Cambridge, Massachusetts, March 1987.

Tappert, F.D., _Wave Propagation and Underwater Acoustics_, Springer-Verlag, Berlin, 1977.

Tolstoy, I., and Clay, C.S., _Ocean Acoustics: Theory and Experiment in Underwater Sound_, American Institute of Physics, Inc., New York, 1987.

Van Trees, L., _Detection, Estimation, and Modulation Theory_, John Wiley & Sons, Inc., New York, 1968.

INITIAL DISTRIBUTION LIST

No. Copies

1. Defense Technical Information Center   2
   Cameron Station
   Alexandria, Virginia   22304-6145

2. Library, Code 0142   2
   Naval Postgraduate School
   Monterey, California   93943-5002

3. Chairman, Code 68   1
   Department of Oceanography
   Naval Postgraduate School
   Monterey, California   93943-5000

4. Chairman, Code 62   1
   Department of Electrical and Computer
     Engineering
   Naval Postgraduate School
   Monterey, California   93943-5000

5. Professor R.H. Bourke, Code 68Bf   2
   Department of Oceanography
   Naval Postgraduate School
   Monterey, California   93943-5000

6. Professor J.H. Miller, Code 62Mr   7
   Department of Electrical and Computer
     Engineering
   Naval Postgraduate School
   Monterey, California   93943-5000

7. Professor G. Cantin, Code 69Ci   1
   Department of Mechanical Engineering
   Naval Postgraduate School
   Monterey, California   93943-5000

8. Commander   1
   Naval Oceanography Command
   NSTL Station
   Bay St. Louis, Mississippi   39522

9. Commanding Officer   1
   Naval Oceanographic Office
   NSTL Station
   Bay St. Louis, Mississippi   39522

10. Commanding Officer   1
    Fleet Numerical Oceanography Center
    Monterey, California   93943

11. Commanding Officer   1
    Naval Ocean Research and Development
      Activity
    NSTL Station
    Bay St. Louis, Mississippi   39522

12. Office of Naval Research, Code 420   1
    Naval Ocean Research and Development
      Activity
    800 North Quincy Street
    Arlington, Virginia   22217

13. Dr. A.B. Baggeroer   1
    Massachusetts Institute of Technology
    Cambridge, Massachusetts   02139

14. Dr. H.P. Bucker   1
    Code 503, Naval Undersea Center
    San Diego, California   92132

15. Monsieur l'Amiral   2
    Chef d'Etat-Major de la Marine
    2, rue Royale
    75200 Paris Naval, France

16. Monsieur le Vice Amiral d'Escadre   2
    Commandant la Force Océanique Stratégique
    75200 Paris Naval, France

17. Monsieur le Contre-Amiral   2
    Attaché Naval près l'Ambassade de France
    4104, Reservoir road NW
    Washington, D.C.   20007

18. Monsieur le Capitaine de Vaisseau   2
    Commandant le CEPMAN
    B.P. 38, 83800 Toulon Naval, France

19. Monsieur, l'Ingenieur en Chef de l'Armement   2
    Directeur de l'EPSHOM
    B.P. 426, 29275 Brest Cedex, France

20. Capitaine de Corvette F. Strohm   5
    ESMED
    83800 Toulon Naval, France

21. Météorologie Nationale   1
    SMM Documentation
    2, avenue Rapp
    75007 Paris, France

22. Professeur J.C. Gascard   1
    Laboratoire d'Océanographie Dynamique
      et Climatologique
    Université Paris 6
    4, place Jussieu
    75252 Paris Cedex 05, France

23. Professeur B. Hamonic   1
    Institut Supérieur
    d'Electronique du Nord
    Département Electronique
    41, Boulevard Vauban
    59046 Lille Cedex, France